

# Nonequilibrium Green Functions in Electronic Device Modeling

Roger K. Lake and Rajeev R. Pandey

Department of Electrical Engineering,

University of California, Riverside, CA 92521-0204

Ph: 951-827-2122; FAX: 951-827-2425; email: rlake@ee.ucr.edu

Jan. 4, 2005

To appear in Handbook of Semiconductor Nanostructures,

American Scientific Publishers,

eds. A. A. Balandin and K. L. Wang

## I. ABSTRACT

We present an overview of electronic device modeling using non-equilibrium Green function techniques. The basic approach developed in the early 1970s has become increasingly popular during the last 10 years. The rise in popularity was driven first by the experimental investigations of mesoscopic physics made possible by high quality semiconductor heterostructures grown by molecular beam epitaxy. The theory has continuously been adapted to address current systems of interest moving from the mesoscopic physics of the late 1980s to single electronics to molecular electronics to nanoscaled FETs. We give an overview of the varied applications. We provide a tutorial level derivation of the polar optical phonon self-energy [1]. Then, focusing on issues of a non-orthogonal basis used in molecular electronics calculations, we derive the basic Green function expressions starting from their definitions in second quantized form in a non-orthogonal basis. We derive the equations of motion for the retarded Green function  $G^R$  and the correlation function  $G^<$ , and we derive the standard expressions for the electron density and the current that are in widespread use. We point out common approximations and open questions of which one finds little discussion in the literature.

## II. INTRODUCTION

The applications of nonequilibrium Green functions [2, 3] have been extensive including quantum optics [4], quantum corrections to the Boltzmann transport equation [5, 6], high field transport in bulk systems [7], and electron transport through nanoscaled systems. Our interest has been in this last category of electron transport through nanoscaled materials under a finite applied bias. Below, we review the work in this area and then provide tutorial derivations of the standard expressions.

Over the last decade, non-equilibrium Green's function (NEGF) techniques have become widely used in corporate, engineering, government, and academic laboratories for modeling high-bias, quantum electron and hole transport in wide variety of materials and devices: III-V resonant tunnel diodes [1, 8, 9, 10, 11, 12, 13, 14, 15, 16, 17, 18, 19, 20, 21, 22, 23], electron waveguides [24], superlattices used as quantum cascade lasers [25], Si tunnel diodes [26, 27], ultra-scaled Si MOSFETs [28, 29, 30, 31, 32], Si nanowires [33, 34, 35], carbon nanotubes [36, 37, 38, 39, 40, 41, 42, 43, 44, 45, 46, 47], metal wires [48, 49], organic molecules [50, 51, 52, 53, 54, 55, 56, 57, 58, 59, 60, 61, 62, 63, 64, 65, 66, 67], superconducting weak links [68], and magnetic leads [38, 69, 70]. Physics that have been included are open-system boundaries [71], full band structure [1, 18, 22, 26, 27, 72], band tails [27], the self-consistent Hartree potential [12, 21, 73], exchange-correlation potentials within a density functional approach [21, 37, 48, 51, 52, 54, 74], acoustic, optical, intra-valley, inter-valley, and inter-band phonon scattering, alloy disorder and interface roughness scattering in Born type approximations [1, 9, 11, 13, 15, 20, 21, 25, 26, 27], photon absorption and emission [25], energy and heat transport [16], single electron charging and nonequilibrium Kondo systems [75, 76, 77, 78, 79, 80, 81], shot noise [14, 17, 82], A.C. [10, 83, 84, 85, 86, 87, 88], and transient response [85, 89]. Time-dependent calculations are described further in [90]. General tutorials can be found in [91, 92].

The general formalism for NEGF calculations of current in devices was first described in a series of papers in the early 1970s [71, 93, 94, 95]. The partitioning of an infinite system into left contact, device, and right contact, and the derivation of the open boundary selfenergies for a tight-binding model was presented in [71]. This theory was re-derived for a continuum representation in [93], tunneling through localized impurity states was treated in [94], and a treatment of phonon assisted tunneling was derived in [95]. In 1976, the formalism was first applied to a multiband model (2-bands) to investigate tunneling [96] and diagonal disorder [97], and in 1980 it was extended to model time-dependent potentials [98].

The citation rate of the first article in the series [71] gives a good indication of the use of the NEGF formalism applied to electronic transport over the last 3 and a half decades. Of the 277 citations listed, 110 occur during the

years from 2000 to the present, 119 occur during the 1990s, 22 citations occur during the 1980s, and 26 citations occur during the 1970s. Over the last decade and a half, the citation rate has been steadily increasing. The motivation for the development of the NEGF tunneling formalism was the metal-insulator-metal tunneling experiments that received much attention during the 1960s [99]. The revival, or accelerated use, of the approach was motivated by the experimental investigations of mesoscopic physics made possible by high quality semiconductor heterostructures grown by molecular beam epitaxy. In 1988, Kim and Arnold appear to be the first to apply the NEGF formalism to such a system, specifically, a resonant tunneling diode [8]. As experimental methods progressed allowing nanomanipulation of matter and probing into the nanoscale regime, the importance of quantum effects and tunneling continuously increased, and the theory adapted to address the current systems of interest moving from mesoscopics to single-electronics to nano-scaled FETs to molecular electronics.

### III. ONE DIMENSIONAL TRANSPORT THROUGH PLANAR SEMICONDUCTOR DEVICES

#### A. NEMO

Effort developing a quantum semiconductor device simulator for devices in which the potential varies along one dimension (1D) through planar semiconductors peaked during Texas Instruments' Nanotechnology Engineering program which ran from 1993-1997 and resulted in the the Nanoelectronic Engineering Modeling (NEMO) program [100]. The Nanoelectronic Engineering Modeling research program was initially conceived to model resonant tunnel diodes (RTDs) and, specifically, to discover the processes that determine the minimum valley current. The program included both theoretical development and software development. Furthermore, somewhat unique to this program, there was a strong experimental verification effort which consisted of the growth, fabrication, and measurement of hundreds of resonant tunnel diodes of varying geometries, layer thicknesses, and material systems forming a large test matrix.

There were several thrusts to the theory and modeling component: (a) a flexible treatment of the open system boundaries [1, 19, 101], (b) charge self-consistency [21, 22, 73] (c) incoherent scattering processes [1, 20, 21, 73, 102] and (d) fullband structure models [22]. An example of a comparison between theory and experiment is shown in Fig. (1). This is a simulation of a GaAs / AlAs RTD with a 5.66 nm well, 3.1 nm barriers, and 20 nm spacer layers at a temperature of 4.2K. The phonon peak is clearly visible. It rides on a background current resulting from interface roughness scattering. The scattering current is calculated self-consistently with the Hartree potential and a local density approximation (LDA) for the exchange-correlation. The magnitude of the scattering assisted valley current matches well the experimental data. It was found that the Hartree potential significantly overestimated the intrinsic bistability [103]. Even with scattering and the LDA potential, the bistability is overestimated since it is observed in the simulations where it is not observed in the experiment.

For room temperature RTDs, simulations indicated that the valley current was determined by thermionic emission through the second resonance for a number of RTDs in the test matrix. A comparison of fullband simulations with experimental data from the test matrix for  $\text{In}_{0.47}\text{Ga}_{0.53}\text{As} / \text{AlAs}$  RTDs and  $\text{In}_{0.47}\text{Ga}_{0.53}\text{As} / \text{In}_{0.48}\text{Al}_{0.52}\text{As}$  RTDs is shown in Figs. (2) and (3). The simulations model purely coherent transport and yet match well with the valley current of the experimental data indicating that at room temperature in these devices, the current is not limited by incoherent scattering. Purely coherent tunneling calculations were never able to match the valley current of notched well RTDs with  $\text{In}_{0.47}\text{Ga}_{0.53}\text{As} / \text{InAs} / \text{In}_{0.47}\text{Ga}_{0.53}\text{As}$  wells [104]. These devices, which have the highest peak-to-valley current ratio of any semiconductor RTD, appear to have their room temperature valley current limited by incoherent scattering.

As the NEMO program progressed, the simulation software was enhanced to model other devices and material systems to support the various experimental programs within TI and Raytheon. One of the important enhancements was the ability to model the Si/SiGe/SiO<sub>2</sub> material system. Fig. (4) shows close agreement between the experimental and simulated capacitance-voltage curve of a metal-oxide-Si (MOS) structure of Barret al. [105] The approach taken for Si for quick design calculations as shown in Fig. (4) was to implement multiple de-coupled single-band models. In these models, Schrodinger's equation is solved independently for each band using Green function techniques. The quantum charge from each calculation is added, and the total is used in the Poisson solver. The quantum calculations and the Poisson calculation are iterated until convergence using a Newton-Raphson algorithm. The simulations of the C-V curve used a 4-independent band model consisting of one band for the 4 equivalent X-valleys, one band for the 2 equivalent X-valleys, one band for the light holes and one band for the heavy holes.

One of the great successes of the NEMO software was its aid in the design of the first working Si/SiGe tunnel diode [106]. There had been significant experimental effort building and testing devices with designs consisting of an 8 nm Si<sub>0.5</sub>Ge<sub>0.5</sub> tunnel region sandwiched between Si. There was delta doping in the Si on either side of the Si<sub>0.5</sub>Ge<sub>0.5</sub> tunnel region and the heavy doping continued through the tunnel region with the n-p junction occurring in the center of the Si<sub>0.5</sub>Ge<sub>0.5</sub>. Several iterations with NEMO lead to a new design with the length of the Si<sub>0.5</sub>Ge<sub>0.5</sub> tunnel region

cut in half from 8 nm to 4nm, and with the doping completely removed from the  $\text{Si}_{0.5}\text{Ge}_{0.5}$  tunnel region. The simulations showed that the delta doping on either side of the 4 nm tunnel region was sufficient to contain the electric field within the tunnel region and the band overlap between the n-conduction band and the p-valence band. The final design simulation is shown in Fig. (5). A decoupled multiple single band model was used. In the strained  $\text{Si}_{0.5}\text{Ge}_{0.5}$  region, the multiple bands are explicitly apparent since they are split in energy by the strain.

### 1. Derivation of the Self-Energies

Ever since its initial publication, there have been continued questions concerning the derivation of the self-energies described in the appendices of [1]. For this reason, we will describe the details of the derivation of the polar-optical phonon self-energy given in Appendix A of [1].

We start with the general form of the electron-phonon potential,

$$V_{ep} = \frac{1}{V} \sum_{\mathbf{q}} U_{\mathbf{q}} e^{i\mathbf{q} \cdot \mathbf{r}} a_{\mathbf{q}} + a_{\mathbf{q}}^{\dagger} \quad (1)$$

where  $\mathbf{q}$  lies within the first Brillouin zone,  $\mathbf{r}$  is the electron coordinate,  $a$  and  $a^{\dagger}$  are the phonon annihilation and creation operators, and  $U_{\mathbf{q}}$  contains the Fourier transform of the electron-ion potential. Details of the derivation of this form of  $V_{ep}$  can be found in Sec. 1.3 of [107].

To second quantize the electron coordinate  $\mathbf{r}$ , we need to define the planar orbital basis and the electron field operators. The planar orbital basis for a zincblende (or diamond) lattice with 2 atoms per unit cell is

$$\begin{aligned} \hat{p}_{i;L;k} &= \frac{1}{N} \sum_{\mathbf{R}_t^L} e^{i\mathbf{k} \cdot \mathbf{R}_t^L} \hat{p}_{i;L;\mathbf{R}_t^L} \\ \hat{c}_{i;L;k} &= \frac{1}{N} \sum_{\mathbf{R}_t^L} e^{i\mathbf{k} \cdot (\mathbf{R}_t^L + \mathbf{v}_t)} \hat{c}_{i;L;\mathbf{R}_t^L} \end{aligned} \quad (2)$$

The anions sit on the Bravais lattice and the cations are offset by the vector  $\mathbf{v} = \frac{a}{4} [111]$ . In the planar orbital basis,  $L$  is the layer index in the [001] direction where a layer includes a layer of anions and a layer of cations and the layer thickness is  $a=2$ ,  $\mathbf{R}_t^L$  is the coordinate in the  $x-y$  plane of the anion in layer  $L$ ,  $\mathbf{R}_t^L + \mathbf{v}_t$  is the coordinate of the corresponding cation in the  $x-y$  plane, and  $\mathbf{k}$  is a 2 dimensional wavevector in  $x$  and  $y$ . The indices  $a_i$  and  $c_i$  label the atomic-like orbitals  $s, p^3, d^5, s^*$  on the anions and cations, respectively. With this basis, the electron field operators are then defined as

$$\psi(\mathbf{r}) = \sum_{k;L} \sum_{a_i} \hat{p}_{i;L;k} c_{a_i;L;k} + \sum_{c_i} \hat{c}_{i;L;k} c_{c_i;L;k} \quad (3)$$

where  $c_{a_i;L;k}$  is the destruction operator for state  $\hat{p}_{i;L;k}$  and  $c_{c_i;L;k}$  is the destruction operator for state  $\hat{c}_{i;L;k}$ .

The second quantized electron-phonon Hamiltonian is then,

$$\begin{aligned} \hat{H}_{ep} &= \frac{1}{V} \sum_{\mathbf{q}} U_{\mathbf{q}} (a_{\mathbf{q}} + a_{\mathbf{q}}^{\dagger}) \int d^3r \psi^{\dagger}(\mathbf{r}) e^{i\mathbf{q} \cdot \mathbf{r}} \psi(\mathbf{r}) \\ &= \frac{1}{V} \sum_{\mathbf{q}} U_{\mathbf{q}} (a_{\mathbf{q}} + a_{\mathbf{q}}^{\dagger}) \sum_{k;k^0;L;L^0} \sum_{a_i;a_i^0} \sum_{c_i;c_i^0} \\ &\quad \left[ h_{a_i;L;k} \hat{p}_{i;L;k}^{iq} \hat{p}_{i^0;L^0;k^0}^0 + h_{c_i;L;k} \hat{c}_{i;L;k}^{iq} \hat{c}_{i^0;L^0;k^0}^0 \right] C_{a_i;L^0;k^0} C_{a_i^0;L^0;k^0}^{\dagger} \end{aligned} \quad (4)$$

$$+ \sum_{a_i;a_i^0} \sum_{c_i;c_i^0} \left[ h_{a_i;L;k} \hat{p}_{i;L;k}^{iq} \hat{p}_{i^0;L^0;k^0}^0 + h_{c_i;L;k} \hat{c}_{i;L;k}^{iq} \hat{c}_{i^0;L^0;k^0}^0 \right] C_{c_i;L^0;k^0} C_{c_i^0;L^0;k^0}^{\dagger} \quad (5)$$

$$+ \sum_{c_i;c_i^0} \sum_{a_i;a_i^0} \left[ h_{c_i;L;k} \hat{c}_{i;L;k}^{iq} \hat{c}_{i^0;L^0;k^0}^0 + h_{a_i;L;k} \hat{p}_{i;L;k}^{iq} \hat{p}_{i^0;L^0;k^0}^0 \right] C_{a_i;L^0;k^0} C_{c_i^0;L^0;k^0}^{\dagger} \quad (6)$$

$$+ \sum_{c_i;c_i^0} \sum_{a_i;a_i^0} \left[ h_{c_i;L;k} \hat{c}_{i;L;k}^{iq} \hat{c}_{i^0;L^0;k^0}^0 + h_{a_i;L;k} \hat{p}_{i;L;k}^{iq} \hat{p}_{i^0;L^0;k^0}^0 \right] C_{c_i^0;L^0;k^0} C_{a_i;L^0;k^0}^{\dagger} \quad (7)$$

To evaluate the matrix elements of  $e^{iq \cdot r}$  in (4) - (7), we must expand out the planar orbitals in terms of the localized orbitals. The anion-anion matrix elements of (4) become

$$\frac{1}{N} \sum_{R_t, R_t^0} \sum_{L, L^0} \sum_{k, k^0} \sum_{a, a^0} e^{ik \cdot R_t} h_{a;L;R_t} e^{iq \cdot R_t} e^{iq \cdot R_t^0} e^{ik^0 \cdot R_t^0} C_{a;L;k}^y C_{a^0;L^0;k^0}^y \quad (8)$$

In the long wavelength approximation, the matrix element in (8) is evaluated as

$$h_{a;L;R_t} e^{iq \cdot R_t} e^{iq \cdot R_t^0} = e^{iq_2 \cdot L} e^{iq_1 \cdot R_t} e^{iq_1 \cdot R_t^0} \quad (9)$$

where  $L = a/2$  is the monolayer (anion plus cation layer) thickness. The phase  $e^{iq \cdot r}$  is evaluated at the position of the anion ( $R_t; L = z$ ) and pulled outside of the integral. The orthogonality of the orbitals results in the Kronecker delta functions. Boykin has shown that, in general,  $r$  is diagonal in the empirical tight-binding basis, so that the evaluation of the matrix element in (9) is true in general and does not rely on the long wavelength approximation [108]. With the matrix evaluated as in (9), term (4) becomes

$$\begin{aligned} & \frac{1}{N} \sum_{L, L^0} \sum_{k, k^0} \sum_{a, a^0} e^{R_t \cdot (q + k^0 - k)} e^{iq_2 \cdot L} C_{a;L;k}^y C_{a^0;L^0;k^0}^y \\ & = \sum_{L, L^0} \sum_{k, k^0} \sum_{a, a^0} e^{iq_2 \cdot L} C_{a;L;k}^y C_{a^0;L^0;k^0}^y \end{aligned} \quad (10)$$

Evaluating the matrix elements as in (9), there will clearly be no matrix elements between anion and cation orbitals, so that terms (5) and (6) are zero. Following the same procedure to evaluate term (7) gives

$$\sum_{L, L^0} \sum_{k, k^0} e^{iq_2 \cdot (L + L^0)} C_{c;L;k}^y C_{c;L^0;k^0}^y \quad (11)$$

The general form for  $\hat{H}_{ep}$  is

$$\hat{H}_{ep} = \frac{1}{V} \sum_q U_q a_q + a_q^y \quad (12)$$

To calculate the self-energy, we calculate the path ordered Green function expanding out the S-matrix in the interaction representation,

$$G_{L;L^0}^P(k;t;t^0) = i \mathcal{P} e^{-i \int_c ds H^0(s)} c_{;L;k}(t) c_{;L^0;k}^y(t^0) i \quad (13)$$

$\mathcal{P}$  is the path ordering operator,  $c$  is the Keldysh contour, and  $H^0(s)$  is the perturbing Hamiltonian, in this case,  $\hat{H}_{ep}$ . The brackets  $\langle \dots \rangle_i$  indicate the nonequilibrium ensemble average [9, 110]. Expanding out the exponential to second order, gives two non-zero terms, the zero order term and the second order term. The first order term is zero since in the absence of interactions,  $h_{q,i} = h_{q,i}^y = 0$ .

The second order term is

$$\begin{aligned} & \frac{i^3}{2V} \sum_{Z, Z^0} \sum_{q_1, q_2} \sum_{L_1, L_2} \sum_{k_1, k_2} \sum_{i, j} e^{iq_{21} \cdot (L_1 + L_2)} e^{iq_{22} \cdot (L_2 + L_1)} \\ & \mathcal{P} \int_c ds_1 \int_c ds_2 a_{q_1}(s_1) + a_{q_1}^y(s_2) a_{q_2}(s_2) + a_{q_2}^y(s_1) \\ & c_{;L_1;k_1}^y(s_1) c_{;L_1;k_1}(s_1) c_{;L_2;k_2}^y(s_2) c_{;L_2;k_2}(s_2) c_{;L;k}(t) c_{;L^0;k}^y(t^0) i \end{aligned} \quad (14)$$

where  $i = 1=2$  if  $i$  is a cation orbital and zero otherwise.

We now apply Wick's Theorem to factor the operators and evaluate them in the absence of interactions [111, 112]. The phonon operators become

$$\begin{aligned} & \mathcal{P} a_{q_1}(s_1) + a_{q_1}^y(s_2) a_{q_2}(s_2) + a_{q_2}^y(s_1) i \\ & = \mathcal{P} a_{q_1}(s_1) a_{q_2}^y(s_2) i + \mathcal{P} a_{q_2}(s_2) a_{q_1}^y(s_1) i / \langle a_{q_1}; a_{q_2} \rangle \end{aligned} \quad (15)$$

The Kronecker delta function arises because the operators are evaluated in the absence of interactions so that the phonon modes are conserved.

There are 2 possible ways to factor the electron operators to give the rainbow diagram, Fig. (12), leading to the standard self-consistent Born approximation. Both factorizations are equivalent canceling the factor of  $1=2$  in Eq. (14). There is also a bubble diagram identical in form to the Hartree self-energy diagram. In bulk, due to momentum considerations, this diagram is exactly zero (p. 401 of Fetter and Walecka [12]). In a heterostructure, this term is not necessarily zero, and it has been investigated in detail by Hyldgaard et al. [13]. We have ignored the bubble diagram and only consider the two equivalent factorizations leading to the self-consistent Born approximation. Choosing one of the two equivalent factorizations, the electron operators become

$$\begin{aligned} & \hbar c_{1L_1; k_1}(t) c_{1L_1; k_1}^\dagger(s_1) i \hbar c_{2L_2; k_2}(s_2) c_{2L_2; k_2}^\dagger(t) \\ & = c_{1L_1; k_1} g_{1L_1}^P(k; t; s_1) c_{2L_2; k_2} g_{2L_2}^P(k; s_2; t) \end{aligned} \quad (16)$$

In (16), a lower case  $g$  is used to indicate the bare Green function in the absence of the electron-phonon interaction. Since the operators are evaluated in the absence of phonon interactions, transverse momentum is conserved giving rise to the Kronecker delta functions.

With the factorization of the electron and phonon operators, the second order term (14) becomes

$$\begin{aligned} & \frac{1}{V} \sum_q \sum_{i,j} e^{iqz} \langle L_1, L_2+1; 2 \rangle \\ & \int_{s_1}^{s_2} ds_1 \int_{s_2}^{s_1} ds_2 \hbar^2 a_q(s_1) a_q^\dagger(s_2) i + \hbar^2 a_q(s_2) a_q^\dagger(s_1) i \\ & g_{1L_1}^P(k; t; s_1) g_{2L_2}^P(k; s_2; t) \end{aligned} \quad (17)$$

where

$$\langle L_1, L_2+1; 2 \rangle = \begin{cases} < \frac{1}{2} & L_1 = c, L_2 = a \\ > \frac{1}{2} & L_1 = a, L_2 = c \\ 0 & \text{otherwise} \end{cases} \quad (18)$$

The general form of the path ordered Dyson's equation resulting from expanding Eq. (13) is

$$\begin{aligned} G_{L; 0L}^P(k; t; t^0) & = g_{L; 0L}^P(k; t; t^0) \\ & + \int_{s_1}^{s_2} ds_1 \int_{s_2}^{s_1} ds_2 G_{L; 1L_1}^P(k; t; s_1) G_{1L_1; 2L_2}^P(k; s_1; s_2) g_{2L_2; 0L}^P(k; s_2; t^0) \end{aligned} \quad (19)$$

Comparing Eq. (19) to Eq. (17), we identify the self-energy as

$$\begin{aligned} \Sigma_{1L_1; 2L_2}^P(k; s_1; s_2) & = \frac{1}{V} \sum_q e^{iqz} \langle L_1, L_2+1; 2 \rangle \\ & \hbar^2 a_q(s_1) a_q^\dagger(s_2) i + \hbar^2 a_q(s_2) a_q^\dagger(s_1) i G_{1L_1; 2L_2}^P(k; s_1; s_2) \end{aligned} \quad (20)$$

In going from Eq. (17) to Eq. (20), we have replaced the bare  $g^P$  with the full  $G^P$  that must be calculated self-consistently with the self-energy  $\Sigma^P$ . This replacement of  $g^P$  with  $G^P$  sums the whole class of rainbow diagrams an example of which is shown in the context of Hartree-Fock theory in Fig. 10.2 of Fetter and Walecka [12].

The real-time self-energies that we need,  $\Sigma^<$ ,  $\Sigma^>$ , and  $\Sigma^R$ , are obtained from  $\Sigma^P$  by considering the individual cases of  $s_1$  and  $s_2$  lying on different branches of the Keldysh contour. Or, one can simply use the relations of Langreth [10]. For pedagogical reasons, we will evaluate  $\Sigma^<$  by considering the time contour and not using the Langreth rules.  $\Sigma^<(s_1; s_2)$  is obtained from  $\Sigma^P(s_1; s_2)$  by considering the case of  $s_2 > s_1$ . According to the path ordering operator  $P$ , the only way that  $s_2$  can always be greater than  $s_1$  is if  $s_2$  lies on the upper branch of the contour and  $s_1$  lies on the lower branch. Applying the path ordering operator, which places operators of later times to the left, to the time dependent terms of Eq. (20), we obtain

$$\begin{aligned} & \hbar^2 a_q^\dagger(s_2) a_q(s_1) i + \hbar^2 a_q(s_2) a_q^\dagger(s_1) i G_{1L_1; 2L_2}^<(k; s_1; s_2) \end{aligned} \quad (21)$$

where

$$G_{1L_1; 2L_2}^<(k; s_1; s_2) = \frac{i}{\hbar} c_{2L_2; k}^\dagger(s_2) c_{1L_1; k}(s_1) i \quad (22)$$

The operators  $a$  and  $a^\dagger$  are evaluated in the absence of interactions. Therefore, their time dependence is

$$\begin{aligned} a_q(s) &= a_q e^{-i\omega_q s} \\ a_q^\dagger(s) &= a_q^\dagger e^{i\omega_q s} \end{aligned} \quad (23)$$

The phonon ensemble averages are evaluated as

$$\begin{aligned} \langle a_q^\dagger a_q \rangle &= n_q \\ \langle a_q a_q^\dagger \rangle &= n_q + 1 \end{aligned} \quad (24)$$

where  $n_q$  is the average phonon number in mode  $q$  which, in equilibrium, is the Bose-Einstein factor. Using (24) and (23), the time dependent terms of (22) become

$$\frac{\hbar}{n_q} e^{-i\omega_q(s_1 - s_2)} + (n_q + 1) e^{i\omega_q(s_1 - s_2)} G_{1L_1; 2L_2}^<(k, \omega; s_1; s_2) \quad (25)$$

In steady state,  $G^<$  is a function of the time difference coordinate  $s_1 - s_2$  which we Fourier transform into energy according to

$$\begin{aligned} \int_{-\infty}^{\infty} d(s_1 - s_2) e^{iE(s_1 - s_2)} \frac{\hbar}{n_q} e^{-i\omega_q(s_1 - s_2)} + (n_q + 1) e^{i\omega_q(s_1 - s_2)} G_{1L_1; 2L_2}^<(k, \omega; s_1 - s_2) \\ = n_q G_{1L_1; 2L_2}^<(k, \omega; E - \omega_q) + (n_q + 1) G_{1L_1; 2L_2}^<(k, \omega; E + \omega_q) \end{aligned} \quad (26)$$

Placing this back into Eq. (20), we obtain the general form for the phonon scattering self-energy within the self-consistent Born approximation.

$$\begin{aligned} \Sigma_{1L_1; 2L_2}^<(k; E) &= \frac{1}{V} \sum_q J_q^2 e^{iqz} (L_1 - L_2 + 1; 2) \\ & n_q G_{1L_1; 2L_2}^<(k, \omega; E - \omega_q) + (n_q + 1) G_{1L_1; 2L_2}^<(k, \omega; E + \omega_q) \end{aligned} \quad (27)$$

The evaluation of  $\Sigma^>$  proceeds in exactly the same way with the difference being that  $s_1 > s_2$  when evaluating the time-dependent terms of Eq. (20). Therefore, the operator ordering is reversed in Eq. (21). The result is

$$\begin{aligned} \Sigma_{1L_1; 2L_2}^>(k; E) &= \frac{1}{V} \sum_q J_q^2 e^{iqz} (L_1 - L_2 + 1; 2) \\ & n_q G_{1L_1; 2L_2}^>(k, \omega; E + \omega_q) + (n_q + 1) G_{1L_1; 2L_2}^>(k, \omega; E - \omega_q) \end{aligned} \quad (28)$$

The relationship of the retarded selfenergy  $\Sigma^R$  to  $\Sigma^<$  and  $\Sigma^>$  is

$$\Sigma^R(t; t^0) = \Sigma^>(t; t^0) - \Sigma^<(t; t^0) = -i \theta(t - t^0) \Sigma^>(t; t^0) \quad (29)$$

or, Fourier transforming the time difference coordinate to energy,

$$\Sigma^R(E) = P \int \frac{dE^0}{2} \frac{\Sigma^>(E^0)}{E - E^0} - \frac{i}{2} \Sigma^>(E) \quad (30)$$

Since  $\Sigma^>(E)$  is Hermitian, the principal value integral is also Hermitian. This term gives rise to an energy renormalization but no relaxation or dephasing. Because the principal value integral is so difficult to perform numerically, this term is often ignored and  $\Sigma^R(E)$  is approximated as  $-\frac{i}{2} \Sigma^>(E)$  where

$$\Sigma^>(E) = -i \Sigma^>(E) - \Sigma^<(E) \quad (31)$$

Another approach, the one implemented in NEMO and described in [1], is to use the single-electron or low-density approximation. In this approximation  $\Sigma^<$  is set to zero since the inscattering into energy  $E - \omega$  is proportional to the electron density  $G^<$  at energies  $E - \omega$ . The electron density is assumed low and thus approximated as equal to zero. The outscattering  $\Sigma^>$  at energy  $E$  is proportional to the hole density  $G^>$  at energies  $E - \omega$ . Since the electron density is zero, the hole density is just the total density of states. Therefore  $G^>$  is replaced in Eq. (28) by  $iA$  where  $A$  is the spectral function. All of the energy dependence of  $\Sigma^>$  is contained in the spectral function. Furthermore, from Eq. (31),  $\Sigma^> = -i \Sigma^R$ . Since  $\Sigma^R$  is related to  $A$  in exactly the same way as  $\Sigma^R$  is related to  $\Sigma$ , Eq. (30) converts

the spectral functions occurring in  $\chi^>$  into retarded Green functions. The retarded self energy then has exactly the same form as  $\chi^>$  Eq. (28) with  $G^R$  replacing  $G^>$ . This form of the self energy does conserve current.

With the general form of the self energy (28), we now consider the specific form of  $U_q$  corresponding to dispersionless polar optical phonons. For dispersionless polar optical phonons,  $n_q = n_0$ ,  $n_q = n_B$  ( $n_0 = 1 = (e^{-\hbar\omega/k_B T} + 1)^{-1}$ ), and

$$J_{qf} = \frac{e^2 n_0}{2} \frac{1}{\epsilon_1} \frac{1}{\epsilon_0} \frac{q^2}{(q^2 + q_0^2)^2} \quad (32)$$

where  $q_0$  is the inverse screening length [14]. For numerical reasons, we prefer to have  $G^>$  in Eq. (28) be only a function of  $q_t$  rather than  $k = q_t$ . Therefore, we change dummy indices so that the expression for  $\chi^>$  becomes

$$\chi^>_{1L_1; 2L_2}(k; E) = \frac{1}{V} \sum_q J_{kq} J^2 e^{iq_z(L_1 - L_2 + 1; 2)} n_B G^>_{1L_1; 2L_2}(q_t; E + \hbar\omega) + (n_B + 1) G^>_{1L_1; 2L_2}(q_t; E - \hbar\omega) \quad (33)$$

When it is appropriate to approximate  $G^>(q_t; E)$  as being independent of the angle of  $q_t$  in the  $x-y$  plane, then we can perform the angular integration analytically. This approximation would be appropriate near the conduction band edge of GaAs where the bands are spherical. The sum over  $q$  becomes the following integral in cylindrical coordinates,

$$\sum_q \frac{dq_x dq_y}{(2\pi)^2} G^>(q; E - \hbar\omega) = \int_0^{z_2} \frac{dq_z}{2} e^{iq_z(L_1 - L_2 + 1; 2)} \int_0^{z_2} d\phi \frac{k q^2}{(k^2 + q^2 + q_0^2)^2} \quad (34)$$

The integral over  $\phi$  is

$$I = \int_0^{z_2} d\phi \frac{k^2 + q_x^2 + q_y^2 - 2kq_x \cos \phi}{(k^2 + q_x^2 + q_y^2 + q_0^2 - 2kq_x \cos \phi)^2} \quad (35)$$

This integral is evaluated by making the substitution

$$z = e^{i\phi} \quad (36)$$

which converts the integral over  $\phi$  into a contour integral around the unit circle. The integral is then evaluated using the residue theorem. With substitution (36), Eq. (35) becomes

$$I = \frac{i}{kq_x} \int_C dz \left[ \frac{1}{z^2 - bz + 1} + \frac{\frac{q_x^2}{kq_x} z}{[z^2 - bz + 1]^2} \right] \quad (37)$$

where

$$b = \frac{k^2 + q_x^2 + q_y^2 + q_0^2}{kq_x} \quad (38)$$

Evaluating (37) with the residue theorem, we obtain

$$I(q_x^2; q_y^2; k^2) = 2\pi \left[ \frac{1}{(q_x^2 + q_y^2 + k^2 + q_0^2)^2} \frac{q_0^2 (q_x^2 + q_y^2 + k^2 + q_0^2)}{4k^2 q_x^2} \right] \quad (39)$$

We write the integral over  $q_x$  in Eq. (34) as

$$\int_0^{z_2} \frac{dq_x}{2} \cos [q_x(L_1 - L_2 + 1; 2)] I(q_x^2; q_y^2; k^2) \quad (40)$$

and the final form of the self energy becomes

$$\chi^>_{\mu L; \nu L^0}(k; E) = \frac{e^2 n_0}{2} \frac{1}{\hbar} \frac{1}{\epsilon_0} \int_0^{z_2} \frac{dq_x^2}{4} I_{\mu L; \nu L^0}(q_x; E + \hbar\omega) + (n_B + 1) G^>_{\mu L; \nu L^0}(q_x; E - \hbar\omega) \quad (41)$$

where

$$I = \int_0^{\pi} \int_0^{\pi} \int_0^{\pi} \cos^2 \alpha \, d\alpha \, d\beta \, d\gamma \int_0^{\infty} \frac{d\alpha}{\alpha} \frac{1}{(\alpha^2 + \alpha_0^2 + k^2 + \alpha_0^2)^2} \frac{4k^2 \alpha^2}{\alpha} \quad (42)$$

Note that the integrand in Eq. (41) is only a function of the magnitude  $\alpha = |\mathbf{j}_t|$ . The integral over the angle was done analytically. We keep the form of the full two dimensional integral because, in an effective mass model, we make the following change of variables,

$$\int_0^{\infty} \frac{d^2 \alpha}{4\pi^2} \int_0^B d\alpha_{\perp} \int_{E_{min}}^{E_z} dE_z \quad (43)$$

where  $\alpha_{\perp}$  and  $E_z$  are defined variables,  $E$  is the total energy,  $B$  is the bandwidth,  $\rho_{2D}$  is the 2D density of states, and  $E_{min}$  is a minimum energy used in the numerical integration.  $\alpha_{\perp}$  is the transverse energy using the dispersion relation in the  $\alpha$  band part of the injecting contact. For a parabolic dispersion,  $\alpha_{\perp} = \frac{\hbar^2 \alpha_{\perp}^2}{2m}$  where  $m_L$  is the effective mass in the injecting contact. Therefore,  $\rho_{2D} = m^{-2}$ . The longitudinal energy is defined as  $E_z = E - \alpha_{\perp}$ .

## B. Post NEMO 1D NEGF Developments

Since its delivery to the U.S. government in 1997, the public availability of NEMO has been sporadic [115]. Currently, NEMO is semi-publicly available with restrictions [116]. Interesting post-NEMO developments of applications for NEGF to 1D transport through planar semiconductor structures are the formulation of NEGF theory to model superlattices and quantum cascade lasers [25] and the application of NEGF theory to model the indirect phonon assisted tunneling in Si tunnel diodes [26, 27].

### 1. Interband, Intervalley Tunneling in Si

The NEGF theory developed to model indirect phonon assisted intervalley, interband tunneling in Si tunnel diodes went back to the original theory of Caroli et al. described in the 4th article of the series [95]. The original theory was rederived for localized orbital full band models with the specific types of phonons important for interband tunneling in Si. A detailed description of the theory is given in [27]. Calculations were performed both with a second nearest neighbor  $sp^3$ s [117] and a nearest neighbor  $sp^3s d^5$  planar orbital basis [118]. The specific phonons of interest were the zone edge TA and TO phonons. From a theoretical and computational point of view, modeling interband tunneling in Si is interesting and challenging because it is primarily an indirect, phonon assisted process. Furthermore, it is an intervalley process in which an electron starts out in one of the 6 valleys near X along the  $\Gamma$  line and tunnels to the valence band at  $\Gamma$ .

The band diagram of the device simulated along with the 6 valleys of the conduction band is shown in Fig. 6. The tunnel current is dominated by the electrons in the 4 transverse valleys whose long axis is perpendicular to the direction of current flow. In the simplest picture, this is because the effective mass in the tunneling direction of the 4 transverse valleys is 5 times lighter than that of the 2 longitudinal valleys, and their combined 2D density of states is 5 times greater. There is a small coherent tunnel current that arises from electrons tunneling from the 2 longitudinal valleys of the conduction band directly to the valence band. This is possible since the transverse wavevector of the electrons in the 2 longitudinal valleys is centered at  $k = 0$  and can therefore be conserved in the coherent tunneling process.

The current modeled has 3 separate components. The coherent component is given by the usual expression [1, 27, 91, 119].

$$J = \frac{e}{A} \sum_k \int \frac{dE}{2} \text{tr} [g_L^R g_R^A f_L^L - f_R^R] \quad (44)$$



In Eq. (44), lower case  $g$  symbols are used for the Green functions since they are the bare Green functions calculated in the absence of phonon scattering. The phonon assisted component of the current is given by [27]

$$\begin{aligned}
 J_1 = & \frac{4e(D_{tK})^2}{!a} \int_x^Z \frac{d^2k_x}{4^2} \int^Z \frac{d^2k}{4^2} \int \frac{dE}{2} \text{tr} a_n^x(k_x; E) \\
 & \text{tr} a_n(k; E \sim!) f^X(E) 1 f(E \sim!) (n_B(\sim!) + 1) \\
 & + \text{tr} a_n(k; E + \sim!) n_B(\sim!) f^X(E) 1 f(E + \sim!) \\
 & \text{tr} a_n(k; E \sim!) 1 f^X(E) f(E \sim!) n_B(\sim!) \\
 & \text{tr} a_n(k; E + \sim!) 1 f^X(E) f(E + \sim!) (n_B(\sim!) + 1) : \quad (45)
 \end{aligned}$$

Eq. (45) is Fermi's Golden Rule written in Green function form. It is a fullband version of Eq. (49) of Caroli et al. [95] written for TO and TA zone edge phonons. To emphasize the intervalley process, subscripts and superscripts  $x$  and  $X$  are used in Eq. (45). The quantity  $a^x$  indicates the left injected spectral function corresponding to Fig. 6. Since it is injected from the left, it is in one of the  $X$  valleys of the conduction band. Similarly,  $a$  indicates the right injected spectral function which is in the valence band near  $\Gamma$ . The integrations over the transverse momenta are performed around the respective valley minimum points. Eq. (45) is evaluated individually for each type of phonon, TO and TA, and the results are added. The relative magnitude of the 3 components can be seen in Fig. 7. Note that the axis for the "Direct" current which is the coherent current is in mA whereas the axis for the phonon assisted current is in A. The magnitude of the coherent current is approximately 5 orders of magnitude smaller than the phonon assisted current.

One issue that was theoretically investigated was to understand the effect of quantized states in the contacts. These formed in the delta-doped wells shown in Fig. 6. The effect of these states was to give some structure to the current-voltage curves primarily in the negative differential resistance (NDR) region as is shown in Fig. 7. The inset of Fig. 7 gives an intuitive explanation of why the structure occurs in the NDR region. The 2D channels are initially on. As they uncross, the channels get turned off giving structure to the I-V. Since the quantum wells are degenerately doped, inclusion of realistic broadening in the calculations completely wipes out any structure in the I-V [26].

A comparison between the experimental and calculated I-V curves is shown in Fig. 8. The discrepancy in the magnitude of the experimental and calculated current (approximately a factor of 5) can be the result of several factors. The magnitude of the current depends quadratically on the magnitude of the deformation potential and exponentially on the width of the tunnel junction and the evanescent wave vector in the tunnel junction. A series of calculations were performed increasing the separation of the delta-doping planes and thus increasing the tunnel junction width. The magnitude of the peak current had a dependence of  $\exp(-d/0.42)$  where  $d$  is the tunnel junction width in nm. For reference, the simplest analytic, parabolic, effective mass model results in a dependence of  $\exp(-d/0.5)$ . The dependence of  $\exp(-d/0.42)$  agreed fairly well with the dependence of  $\exp(-d/0.38)$  extracted from reverse biased Si pn junctions from a later exhaustive experimental study [120].

The decay lengths are determined by the evanescent wavevectors in the bandgap. The full band calculations are compared with the parabolic effective mass model in Fig. 9. The full band calculations result in evanescent wavevectors in the gap that are smaller than that of the parabolic effective mass model. This is to be expected since the evanescent hole bands wrap around to an excited band above the conduction band and the evanescent electron bands near  $X$  wrap around to a hole band near  $X$ . The surprising thing is that in the simple analytical tunneling model, the smaller evanescent wavevector should result in a decay length larger than the effective mass model when in fact the current calculations show the opposite. This apparent contradiction is not understood.

## 2. Quantum Cascade Lasers

The most comprehensive application of NEGF theory to superlattices and quantum cascade lasers was presented in Lee and Wacker [25] which built upon previous work [121, 122, 123]. The difficulty with modeling quantum cascade lasers is that they are very long containing 40 or more periods of active and injector regions under large bias and a treatment of scattering is essential since the transport through the structure is all scattering assisted. Lee and Wacker reformulated NEGF theory to model these types of structures as shown in Fig. 10. Their formulation of NEGF theory takes a radical departure from all of the other work discussed in this chapter [25]. All of the other work is based on a formulation of NEGF theory that has the work of Caroli et al. [71] as its foundation. In particular all of the other work partitions the infinite system into a "device" which is the system of interest and contacts which act as thermal reservoirs for electrons and the partitioning is done as first described in [71]. In the formulation of NEGF theory by Lee and Wacker, there are no contact regions. Special "periodic" boundary conditions are used in which the Green

functions and selfenergies satisfy

$$G_{i^0,j^0}(E - qV) = G_{i,j}(E) \quad (46)$$

In Eq. (46),  $i$  and  $j$  are the localized Wannier function index within one period of the structure,  $E$  is the total energy, and  $V$  is the voltage drop across one period of the structure. Everything is periodic but shifted down in energy by the voltage drop across one period.

Since there are no contacts in this theory, an expression for current density cannot be obtained by considering current flow from the contact to the device. Instead, an expression for the current density is obtained by evaluating

$$J(t) = \frac{e}{V} \frac{d\hat{z}}{dt} \hat{z} = \frac{e}{V} \frac{1}{\hbar} \hat{z} \hat{H} \hat{z} \quad (47)$$

The Hamiltonian is then broken up into an unperturbed part  $H_0$  and a scattering part  $H^0$ . The unperturbed part gives rise to the standard current expression

$$J_0 = \frac{e}{\sim A} \frac{1}{k} \sum_k \frac{dE}{2} \text{tr} \left[ t_{i,i+1} G_{i+1,i}^< - t_{i+1,i} G_{i,i+1}^< \right] \quad (48)$$

where the matrices  $t$  and  $G^<$  are in the basis of Wannier functions, the trace is over all Wannier functions and spin within a period,  $t$  is the off-diagonal Hamiltonian matrix coupling Wannier functions between periods  $i$  and  $i+1$ ,  $k$  is the transverse wavevector, and  $A$  is the cross-sectional area. We have used the fact that  $\hat{z}$  is diagonal in the Wannier basis. This equation is equivalent in form to Eq. (18) and (22) of Caroli et al. [71] derived from the electron continuity equation, Eq. (20) of Lake et al. [1], Eq. (20) of Svizhenko and Anantram [31], and Eq. (132) derived later in this chapter.

What is particularly interesting is that the scattering component of the Hamiltonian in Eq. (47) results in a current term

$$J_{\text{scatt}} = \frac{e}{\sim V} \frac{1}{k} \sum_k \frac{dE}{2} \text{tr} \left[ z G^< A + G^R < - < G^A - R G^< \right] \quad (49)$$

This is the first time of which we are aware that such a term has been derived. In a basis in which  $z$  is diagonal, for example the Wannier basis or the empirical tight binding basis analyzed by Boykin [108], Eq. (49) reduces to

$$J_{\text{scatt}} = \frac{e}{\sim A} \frac{1}{k} \sum_k \frac{dE}{2} \text{tr} \left[ G^< A + G^R < - < G^A - R G^< \right] \quad (50)$$

Under very general conditions, it can be shown that this term is equal to zero. See for example Sec. 2.4 of [6] or Eq. (67) of [1].

#### IV. TWO DIMENSIONAL TRANSPORT IN TRANSISTORS

The primary objective for the development of quantum semiconductor device simulators in which the potential varies in two dimensions (2D) is the modeling of ultra-scaled Si based FETs [28, 29, 30, 31]. As the device size and dimension increase, computational intensity increases, and the sophistication of the model must decrease. The 2D simulators treat the bandstructure in a multiple single-band model which includes 3 decoupled bands to account for the three non-equivalent valleys in the quantized channel for NMOS. The simulators have included Hartree quantum charge self-consistency, and open system boundary conditions at the source, drain, and gate. For full 2D quantum transport, empirical, elastic, incoherent scattering models have been implemented [30, 32]. The 2D problem has been further simplified by using mode-space models [32, 124].

True inelastic scattering has been included in a multiple subband model in which the subbands are only coupled through the phonon scattering [31]. Thus, the quantum calculations were reduced to multiple 1D calculations greatly reducing the computational burden. This model was used to simulate the energy relaxation of electrons from dispersionless deformation potential optical phonon scattering in SiGe-type Intervalley scattering was included from phonons with energies of 12, 19, and 62 meV. The electron phonon interaction was treated in the self-consistent Born approximation, and the resulting quantum charge density was iterated self-consistently with a 2D Poisson's equation to convergence.

Dispersionless, deformation potential optical phonon scattering results in a self-energy that is local in position. In ref. [31], the spatial scattering region was increased starting initially in the source, then moving through the

extension and channel, and finally into the drain to encompass the entire FET. The effect of inelastic scattering in various regions of the device is shown in Fig. (11). The particular dual-gate device modeled for this figure has a 10 nm channel, 1.5 nm channel thickness, and 1.5 nm oxide. The gate region lies between 5 nm. As the scattering region is extended through the device from source to drain, the effect on the current is almost symmetric around the center of the channel. This indicates that for ultra-scaled FETs, scattering in the drain end is just as important as scattering in the source end. This contradicts the conclusion of Lundstrom and Ren that "scattering in a short region near the beginning of the channel limits the on-current [125]." The reason for the importance of drain-end scattering in the 10 nm FET is that the gate length is comparable to the scattering length so that hot electrons from the drain-end can be reflected back into the channel. As far as we are aware, this calculation was the first to predict these results.

The largest scale simulations of a 2D FET have been performed by Jovanovic [30]. He performed full 2D simulations of both the MIT 90 nm and 25 nm bulk MOSFETs [30, 126]. An elastic, empirical scattering model was used and calibrated to mobility data. For the 90 nm device, NEGF simulations, drift-diffusion simulations, and experimental data were all essentially indistinguishable. However, the drift-diffusion and NEGF calculations diverge significantly for the 25 nm device. The differences arise from the threshold voltage shift due to the shape of the quantum charge distribution in the channel and tunneling through the gate region.

### 3. Recursive Green Function Algorithm for $G^<$

One of the significant algorithmic developments of the 2D codes was the use of the recursive Green function algorithm (RGFA) for  $G^<$  [29, 30]. The algorithm was first developed during the NEMO program [127] and implemented in early prototypes of the NEMO code, but it did not make it into the final deliverable; only the recursive Green function algorithm for  $G^R$  was used [1]. In ref. [29] the algorithm was used for coherent transport. In ref. [30], the algorithm was used for transport in the presence of incoherent scattering. This was the first use of which we are aware of a recursive Green function algorithm used in the presence of incoherent scattering. It was developed to meet the intense computational demands of modeling the large 90 nm and 25 nm MIT bulk MOSFET devices. Below we give an overview of the algorithm.

First, we note that for elastic incoherent scattering,  $G^<$  can be factored into components injected from the left and right contacts. This can be seen from Eqs. (73) – (76) of ref. [1] or Eq. (13) of [30]. The empirical scattering model has a local, diagonal form for the self energies,

$$\Gamma_{i,j}^R = \delta_{i,j} \quad (51)$$

$$g_{i,j}^< = \frac{t_{i,j}}{A_{i,j}} G_{i,j}^< \quad (52)$$

The form for  $g^<$  conserves current. The general form for  $G^<$  is

$$G^< = G^R g^< G^A + G^R g^< B G^A \quad (53)$$

The first term on the right is from incoherent scattering, and the second term on the right is a source term due to injection from the contacts. The starting point for the RGFA for  $G^<$  is the equation for the left connected  $g^<$

$$g_{i,j}^< = g_{i,j}^R \delta_{i,j}^s + t_{i,j} g_{i-1,j-1}^< t_{i-1,j} g_{i,j}^A \quad (54)$$

The superscripts  $^s$  and  $^a$  are used to indicate whether the semi-infinite portion of  $g^<$ ,  $g^R$ ,  $g^A$ , or  $a^s$  extends towards the left (source) or right (drain) side, respectively.  $\delta_{i,j}^s = \frac{t_{i,j}}{A_{i,j}} G_{i,j}^<{}^s$  and  $G_{i,j}^<{}^s = i f^s A_{i,j}^s$  where the superscript  $s$  indicates source. Writing the equivalent equation for  $g^>$  and subtracting gives an equation for the left connected source spectral function

$$a_{i,j}^s = g_{i,j}^R \frac{t_{i,j}}{A_{i,j}} A_{i,j}^s + t_{i,j-1} a_{i-1,j-1}^s t_{i-1,j} g_{i,j}^a \quad (55)$$

and, similarly, the right connected source spectral function

$$a_{i,j}^s = g_{i,j}^R \frac{t_{i,j}}{A_{i,j}} A_{i,j}^s + t_{i,j+1} a_{i+1,j+1}^s t_{i+1,j} g_{i,j}^a \quad (56)$$

The left connected source spectral function is connected to the source contact. The right connected source spectral function is not connected to either the source or the drain. It is only non-zero if there is incoherent scattering, i.e. if  $\Gamma$  is non-zero. With the right and left connected source spectral functions, the full source spectral function is calculated from

$$A_{i,j}^s = G_{i,j}^r \frac{A_{i,j}^s}{A_{i,j}} + t_{i,j} a_{i-1,j-1}^s t_{i-1,j} + t_{i,j+1} a_{i+1,j+1}^s t_{i+1,j} G_{i,j}^a \quad (57)$$

The above 3 equations must be iterated until convergence at which point current is conserved.

## V. THREE DIMENSIONAL TRANSPORT THROUGH CNTS, NANOWIRES, AND MOLECULES

Three dimensional (3D) modeling has been applied to semiconductor nanowires, carbon nanotubes, and molecules. In all of the 3D applications of which we are aware, the transport is modeled as coherent throughout the nanowire, CNT, or molecule. This may be a good approximation in CNTs, but for electrons traveling through the HOMO or LUMO bands of molecules, the approximation is open to question. The 3D modeling can be roughly classified into two categories. In the first category, the Hamiltonian is constructed using an empirical tight binding model. For well-understood materials such as the common semiconductors, Si, Ge, and GaAs, and carbon nanotubes (CNTs), the empirical models can be highly accurate since they are fitted to known properties of the materials such as band gaps and effective masses [118, 128]. In fact, for semiconductors, the empirical models are more accurate than the ab-initio models. Carbon nanotubes have been extensively modeled using the  $\sigma$ -bond model [47, 129, 130, 131]. In the  $\sigma$ -bond model, the basis consists of one  $p_z$  orbital per atom perpendicular to the axis of the nanotube [132]. The 3D CNT problem has also been simplified by assuming cylindrical symmetry and using a mode-space model [131]. Applications of NEGF to 3D modeling of semiconductors have been more scarce. Both a full-band  $sp^3d^5s$  model and a discretized single band effective mass model were used to calculate transmission coefficients through Si nanowires [33, 34, 35]. No attempt has yet been made to combine the NEGF calculation with a self-consistent Poisson solver and calculate I-V characteristics of the Si nanowires under bias.

In the second category, the Hamiltonian is constructed using ab initio models with density functional theory (DFT) and a localized orbital basis [37, 38, 39, 40, 42, 43, 51, 52, 53, 54, 58, 59, 60, 61, 62, 64, 65, 66, 74]. In this category, NEGF has been integrated with existing codes such as the quantum chemistry code Gaussian98 [51, 52, 54, 74], the computational materials codes SIESTA [48, 133] and FIREBALL [134], and custom codes [37, 59]. It is in this last, highly interdisciplinary category that we find some of the most interesting recent developments.

The general field of molecular electronics has brought together quantum chemists, physicists, material scientists, and electrical engineers. The two primary fields from which theoretical approaches have been taken are solid state physics and computational quantum chemistry. Diagrammatic perturbation theory, Green's functions, and Dyson's equation are the foundation of much of modern solid state physics theory, and it is the basis for non-equilibrium Green function theory [3, 107, 112]. Diagrammatic perturbation theory has had less usage in modern quantum chemistry [135, 136]. Conversely, non-orthogonal basis sets are often used in chemistry [137, 138], but are generally only considered in physics by those working on computational material properties using a localized orbital basis [139, 140, 141, 142, 143, 144, 145]. One exception is Feynman's derivation of the anticommutation properties of creation and annihilation operators in a non-orthogonal basis [146]. The derivations in the literature describing the integration of DFT with NEGF are extensive [37, 48, 51, 52, 54, 74], although there has been little discussion of the validity of DFT in non-equilibrium [53, 147]. Recent work suggests that the breakdown of this approximation may be the reason for the often observed large discrepancy between theoretical and experimental current magnitudes [147]. Also, the derivations make little use of second quantized operators which are the natural language of Green function and diagrammatic perturbation theory [3, 107, 112].

Below, we provide tutorial level derivations of standard expressions starting from their basic definitions in second quantized form in a non-orthogonal basis for an effective single particle Hamiltonian. The focus will be on the new problems that arise when working in a non-orthogonal basis as compared to an orthogonal basis. We will point out open questions and standard approximations of which one finds little discussion in the literature.

## VI. GREEN FUNCTIONS IN A NON-ORTHOGONAL BASIS

## A. The Non-Orthogonal Localized Orbital Basis

We start with a non-orthogonal localized orbital basis  $\{j_i\}$  where the states correspond to the wavefunctions  $\psi_j(\mathbf{r}) = \langle \mathbf{r} | j_i \rangle$ . We next define the biorthogonal basis  $\{j_j\}$  such that

$$\langle j_i | j_j \rangle = \delta_{ij} \quad (58)$$

The overlap matrix is defined as  $S_{ij} = \langle j_i | j_j \rangle$ . By inspection, the orbitals  $\{j_j\}$  are written as linear combinations of the  $\{j_i\}$  as

$$|j_j\rangle = \sum_p S^{-1}_{pj} |j_p\rangle \quad (59)$$

since this satisfies Eq. (58). With the expansion (59), we can calculate the inner product

$$\langle j_i | j_j \rangle = \sum_q S^{-1}_{iq} \langle j_i | \sum_p S^{-1}_{pj} |j_p\rangle = S^{-1}_{ij} = S^{-1}_{ij}$$

The last equality results from the fact that the inverse of a Hermitian matrix is also Hermitian.

In our non-orthogonal basis  $\{j_i\}$ , the identity operator is

$$\hat{I} = \sum_{ij} |j_i\rangle \langle j_j| S^{-1}_{ij} = \sum_j |j_j\rangle \langle j_j| = \sum_j |j_j\rangle \langle j_j| \quad (60)$$

This is proven by sandwiching the identity operator between any two basis states,

$$\langle j_k | \hat{I} | j_l \rangle = \sum_{ij} \langle j_k | j_i \rangle S^{-1}_{ij} \langle j_j | j_l \rangle = \delta_{kl}$$

We next define the creation,  $a_i^\dagger$ , and annihilation,  $a_i$ , operators for the non-orthogonal basis states  $\{j_i\}$  in the usual way such that  $a_i^\dagger$  creates a particle in the empty state  $|j_i\rangle$ . In other words, starting from the vacuum state,  $|0\rangle$ , the single particle state  $|j_i\rangle$  is yielded by applying the creation operator,

$$a_i^\dagger |0\rangle = |j_i\rangle \quad (61)$$

The anti-commutation relations are [146]

$$\{a_i, a_j^\dagger\} = S_{ij} \quad (62)$$

and  $\{a_i, a_j\} = \{a_i^\dagger, a_j^\dagger\} = 0$ . We also define the creation,  $b_j^\dagger$ , and annihilation,  $b_j$ , operators for the bi-orthogonal basis states  $\{j_j\}$  such that

$$b_j^\dagger |0\rangle = |j_j\rangle \quad (63)$$

Substituting the expansion of state  $|j_i\rangle$  in terms of states  $|j_j\rangle$ , Eq. (59), into the right hand side of Eq. (63), and then substituting in Eq. (61) for  $|j_j\rangle$ , we obtain the transformations between the 2 sets of operators,

$$\begin{aligned} b_j^\dagger &= \sum_p S^{-1}_{pj} a_p^\dagger \\ b_j &= \sum_p S^{-1}_{jp} a_p \end{aligned} \quad (64)$$

With these expansions and Eq. (62), it is straightforward to calculate the anti-commutation relations

$$\{b_i, b_j^\dagger\} = S^{-1}_{ij} \quad (65)$$

$$\{a_i, b_j^\dagger\} = \{a_i^\dagger, b_j\} = \delta_{ij} \quad (66)$$

and  $f b_i; b_j g = f b_i^y; b_j^y g = f a_i; b_j g = f a_i^y; b_j^y g = 0$ .

We also introduce the standard field operators,  $\psi(r)$  and  $\psi^\dagger(r)$ , which are the creation and annihilation operators corresponding to the orthonormal position eigenstates  $|j\rangle$ . A particle in state  $|j\rangle$  is created by

$$\psi^\dagger(r)|j\rangle = |j\rangle \quad (67)$$

These have the standard anti-commutation relations,  $\{\psi^\dagger(r^0), \psi(r^0)\} = \delta(r - r^0)$ . By applying the identity operator, Eq. (60), to the right hand side of Eq. (67),

$$\begin{aligned} |j\rangle &= \sum_i |j\rangle \langle i| S^{-1} \sum_{i,j} h_{ij} |j\rangle \\ &= \sum_{i,j} |j\rangle \langle i| S^{-1} \sum_{i,j} \psi_j^\dagger(r) \\ &= \sum_j |j\rangle \psi_j^\dagger(r) \end{aligned} \quad (68)$$

and then expanding the state  $|j\rangle$  using Eq. (61), we obtain the field operators in terms of the localized orbital operators,

$$\begin{aligned} \psi^\dagger(r) &= \sum_i a_i^y S^{-1} \sum_{i,j} \psi_j^\dagger(r) \\ &= \sum_j b_j^y \psi_j^\dagger(r) \end{aligned} \quad (69)$$

Similarly

$$\psi(r) = \sum_j \psi_j(r) b_j \quad (70)$$

It is useful to introduce the 3 different kinds of matrix elements of any operator [139]. We will use the identity operator as an example. The covariant matrix elements are

$$\langle i|\hat{I}|j\rangle = \delta_{i,j} \quad I_{i,j} \quad (71)$$

In other words, the overlap matrix is the covariant representation of the identity operator. The contravariant matrix elements are

$$\langle i|\hat{I}|j\rangle = S^{-1} \delta_{i,j} \quad I^{i,j} \quad (72)$$

The inverse of the overlap matrix is the contravariant representation of the identity operator. The mixed representation of the identity operator is the usual identity matrix,

$$\langle i|\hat{I}|j\rangle = \delta_{i,j} \quad I_j^i \quad (73)$$

where  $\delta_{i,j}$  is the usual Kronecker delta function. These representations of the identity operator act like the metric tensor and serve to raise and lower indices, e.g.,

$$\sum_j I_{i,j} I^{j,k} = I_i^k \quad (74)$$

From Eqs. (59) and (64), we see that the states  $f|j\rangle$  and the creation operators  $b_j^y$  transform in the same way as contravariant quantities. If we were to use superscripts and subscripts to differentiate between the covariant and contravariant states, we could re-write Eq. (59) as

$$|j\rangle = \sum_p |p\rangle I^{p,j} \quad (75)$$

From Eqs. (69) and (70), we see that the field operators are contractions of a covariant and contravariant quantity and are thus independent of the localized orbital basis as they must be. We find this to be a useful check when performing derivations that any operator corresponding to an observable is a fully contracted product of covariant and contravariant quantities.

B. Non-equilibrium Green functions and correlation functions

We will now derive expressions for the electron density and the current in terms of the relevant Green function quantities. Two correlation functions, 2 Green functions, and 1 spectral function are of particular interest. The 2 correlation functions are defined by

$$G_{ij}^<(t;t^0) = \frac{i}{\hbar} \langle b_j^y(t^0) b_i(t) \rangle \quad (76)$$

$$G_{ij}^>(t;t^0) = \frac{i}{\hbar} \langle b_i(t) b_j^y(t^0) \rangle \quad (77)$$

The retarded and advanced Green functions are defined by

$$\begin{aligned} G_{ij}^R(t;t^0) &= (t-t^0) \frac{i}{\hbar} \langle b_i(t) b_j^y(t^0) + b_j^y(t^0) b_i(t) \rangle \\ &= (t-t^0) [G_{ij}^>(t;t^0) - G_{ij}^<(t;t^0)] \end{aligned} \quad (78)$$

$$G_{ij}^A(t;t^0) = (t^0-t) \frac{i}{\hbar} \langle b_i(t) b_j^y(t^0) + b_j^y(t^0) b_i(t) \rangle \quad (79)$$

The spectral function is defined by

$$A_{ij}(t;t^0) = \frac{1}{\hbar} \langle b_i(t) b_j^y(t^0) + b_j^y(t^0) b_i(t) \rangle \quad (80)$$

$$= i [G_{ij}^R(t;t^0) - G_{ij}^A(t;t^0)] \quad (81)$$

$$= i [G_{ij}^>(t;t^0) - G_{ij}^<(t;t^0)] \quad (82)$$

where the brackets  $\langle \dots \rangle$  indicate the non-equilibrium ensemble average [9, 110, 111], and the creation and annihilation operators are in the Heisenberg representation. We will be concerned with steady state in which case the time dependence becomes only a function of  $(t-t^0)$  and is Fourier transformed to energy, e.g.

$$G_{ij}^<(E) = \int dt (t-t^0) e^{iE(t-t^0)} G_{ij}^<(t;t^0) \quad (83)$$

Note that these Green functions, being products of two contravariant quantities, are the contravariant representation of the Green function. It is this representation which is most useful for numerical computations. We will see that  $G_{ij}^R(E)$  is given by the inverse of the matrix whose elements are the covariant representation of  $[E-H]$ , i.e. the inverse of the matrix whose elements are  $\langle b_i | [E-H] | b_j \rangle = E S_{ij} - H_{ij}$ . This matrix is sparse and therefore desirable for numerical manipulation.

The expression for the electron density is straightforward to obtain, and it is directly related to  $G^<$ .

$$\begin{aligned} \langle \hat{n}(r) \rangle &= \langle \sum_X b_X^y(r) b_X(r) \rangle \\ &= \langle \sum_{ij} b_j^y b_i \rangle_{ij}(r) \quad (r) \\ &= i \sum_{ij} \langle G_{ij}^<(t=t^0=0) \rangle_{ij}(r) \quad (r) \\ &= i \sum_{ij} \int_{-\infty}^{\infty} \frac{dE}{2} G_{ij}^<(E) \quad (r) \quad (r) \end{aligned} \quad (84)$$

The expression for the current is less straightforward and we will defer its derivation until we have the equations of motion for  $G^<$  and  $G^R$ .

The equations of motion for the Green functions are derived by applying  $i\hbar \frac{\partial}{\partial t}$  to expressions (76) - (78) and evaluating.

$$i\hbar \frac{\partial}{\partial t} \langle b_j^y(t^0) b_i(t) \rangle = \langle b_j^y(t^0) b_i; \hat{H} \rangle \quad (85)$$

where the effective single particle Hamiltonian is

$$\hat{H} = \sum_{ij} H_{ij} b_i^y b_j \quad (86)$$

The commutator in (85) is evaluated using the anticommutation relation Eq. (66).

$$b_i; \hat{H} = \sum_{k;l} H_{k;l} b_l; b_k^\dagger b_l = \sum_{k;l} S^{-1}_{i;k} H_{k;l} b_l(t) \quad (87)$$

Placing this back into Eq. (85) gives

$$i\hbar \frac{\partial}{\partial t} G_{i;j}^<(t;t^0) = \sum_{k;l} S^{-1}_{i;k} H_{k;l} G_{l;j}^<(t;t^0) \quad (88)$$

Going through the same exercise for  $G_{i;j}^>(t;t^0)$  results in the same equation of motion as for  $G_{i;j}^<(t;t^0)$ . Applying  $i\hbar \partial/\partial t$  to the retarded Green function, Eq. (78), gives

$$i\hbar \frac{\partial}{\partial t} G_{i;j}^R(t;t^0) = (t-t^0) S^{-1}_{i;j} + \sum_{k;l} S^{-1}_{i;k} H_{k;l} G_{l;j}^R(t;t^0) \quad (89)$$

Multiplying through by  $S$  gives

$$i\hbar \sum_1 S_{i;l} \frac{\partial}{\partial t} G_{l;j}^R(t;t^0) = (t-t^0) S^{-1}_{i;j} + \sum_1 H_{i;l} G_{l;j}^R(t;t^0) \quad (90)$$

or in matrix notation

$$i\hbar S \frac{\partial}{\partial t} [H] G^R(t;t^0) = 1(t-t^0) \quad (91)$$

Fourier transforming to energy as in Eq. (83) results in

$$[E S - H] G^R(E) = 1 \quad (92)$$

Similarly, Eq. (88) becomes

$$[E S - H] G^<(E) = 0 \quad (93)$$

### C. Boundary self-energies

#### 1. $G^R$ and $G^<$

Now one partitions the infinite system into a finite "device" region and "contact" regions [1, 71, 91, 148]. Traditionally, one then includes the effect of the "contacts" on the "device" exactly using time dependent diagrammatic perturbation theory summed to all orders to obtain the Dyson's equations for each type of Green function [1, 71, 148]. Time dependent perturbation theory is for perturbations in the Hamiltonian which cause the states to evolve according to unitary transformations. We will see that now we need to also include a perturbation in the off-diagonal elements of the overlap matrix. This, in effect, alters the basis states and thus the Hilbert space spanned by the states. Therefore, it is not clear to us how to incorporate this into the formal nonequilibrium Green's function theory. What we will do is what many others have done [37, 48, 51, 52, 54, 74, 91, 139], which is to use matrix algebra to write an effective Dyson equation for  $G^R$  to include the effect of the contacts. This is an application of inversion by partitioning [149].

We illustrate the concept with a concrete example of a periodic chain of atoms with nearest neighbor overlap of the atomic-orbital-like basis states. Atoms  $f_1, \dots, f_0$  lie in the left contact. Atoms  $f_1, \dots, f_N$  lie in the "device" and atoms  $f_{(N+1)}, \dots, f_1$  lie in the right contact. The matrix elements of the Hamiltonian group into intra-atomic subblocks  $D_{i;i}$  and inter-atomic subblocks  $t_{i;i-1}$ . The size of these matrices is equal to the number of orbitals per atom. In the matrix  $[E S - H]$ , the matrix elements of the left contact couple to those of the device by the off-diagonal blocks

$$[E S - H]_{1,0} = \begin{matrix} \vdots \\ t_{1,0} \end{matrix} \quad (94)$$

and

$$[E S - H]_{0,1} = \begin{matrix} \vdots \\ t_{0,1} \end{matrix} \quad (95)$$



The matrix elements of the right contact couple to those of the device by the off-diagonal blocks

$$E S_{N, N+1} \quad t_{N, N+1} \equiv t_{N, N+1} \quad (96)$$

and

$$E S_{N+1, N} \quad t_{N+1, N} \equiv t_{N+1, N} \quad (97)$$

For any atoms  $i, j \in \{1, \dots, N\}$  in the device, we can write the standard Dyson equation for the retarded Green function using  $t$  in place of  $\tau$ .

$$G_{i,j}^R = g_{i,j}^R + g_{i,1}^R t_{1,0} G_{0,j}^R + g_{i,N}^R t_{N, N+1} G_{N+1,j}^R \quad (98)$$

where  $g^R$  is the "bare" Green function of the uncoupled device, and the energy argument is suppressed. We write a second Dyson equation for the exact  $G_{0,j}^R$  and  $G_{N+1,j}^R$  which cross the device-contact boundaries.

$$G_{0,j}^R = g_{0,0}^R t_{0,1} G_{1,j}^R \quad (99)$$

$$G_{N+1,j}^R = g_{N+1, N+1}^R t_{N+1, N} G_{N,j}^R \quad (100)$$

where  $g_{0,0}^R$  is the "bare" Green function of the end block of the uncoupled left contact (also referred to as the "surface" Green function), and  $g_{N+1, N+1}^R$  is the "bare" Green function of the uncoupled right contact. These are generally calculated from the eigenmodes of the bulk contact regions [27, 35, 54, 91]. Combining Eqs. (98), (99), and (100) gives the standard Dyson equation for the device Green function.

$$G_{i,j}^R = g_{i,j}^R + g_{i,1}^R \underbrace{t_{1,0} g_{0,0}^R t_{0,1}}_{\substack{R B \\ 1;1}} G_{1,j}^R + g_{i,N}^R \underbrace{t_{N, N+1} g_{N+1, N+1}^R t_{N+1, N}}_{\substack{R B \\ N;N}} G_{N,j}^R \quad (101)$$

The retarded self-energies resulting from coupling to the left and right contacts are, respectively,

$$\Sigma_{1;1}^{R B} = (t_{1,0} \quad E S_{1;0}) g_{0,0}^R (t_{0,1} \quad E S_{0;1}) \quad (102)$$

$$\Sigma_{N;N}^{R B} = (t_{N, N+1} \quad E S_{N, N+1}) g_{N+1, N+1}^R (t_{N+1, N} \quad E S_{N+1, N}) \quad (103)$$

We add the superscript B to indicate that these self-energies result from the open-system boundary conditions of the device, and they are not the result of dissipative processes within the device. Multiplying Eq. (101) by the  $N \times N$  block matrix of the isolated device,  $[E S_0 \quad H_0] = g^R$ , results in standard equation for the device Green function.

$$[E S_0 \quad H_0] \Sigma^{R B} G^R = 1 \quad (104)$$

where  $\Sigma^{R B}$  has two nonzero blocks,  $\Sigma_{1;1}^{R B}$  and  $\Sigma_{N;N}^{R B}$ .

At this point, we have derived the matrix equation for the contravariant retarded Green function, Eq. (92), using the Heisenberg equation of motion, Eq. (85), and then we used matrix algebra to determine the values of  $G_{i,j}^R$  in the central device region in terms of the surface Green functions of the contacts, Eq. (104). So far, we have not needed to know anything about time contours and nonequilibrium Green function theory.

## 2. $G^<$ and $G^<^B$

To calculate physical observables such as the electron density and current, we need  $G^<$ . To obtain  $G^<$ , we need an expression for the self-energy  $\Sigma^{< B}$ . This cannot be obtained without recourse to NEGF theory. However, as we noted above, perturbation of the basis states does not appear to be compatible with formal NEGF theory. We will

have to choose a form for  $\langle^B$  that appears to be consistent with the NEGF theory, that is physically reasonable, that satisfies the usual relations between  $G^R$ ,  $\langle^B$ , and  $\rangle^B$ , and that reduces to the correct form in equilibrium.

Once  $\langle^B$  is fixed, Eqs. (102) and (103), certain relationships between the various self-energies must be satisfied such as

$$\langle^B = \frac{\hbar}{i} \text{Im} G_{RB}^R = \frac{\hbar}{i} \text{Im} G_{RB}^A = \langle^B : \quad (105)$$

Furthermore, in equilibrium,  $\langle^B$  is completely determined by  $G_{RB}^R$  from the relation

$$\langle^B = i f G_{RB}^R \quad (106)$$

where  $f$  is the Fermi factor. These two relations considerably limit the possible forms for  $\langle^B$ . One also finds the argument in the literature that since the contacts are in equilibrium,  $\langle_{1;1}^B$  must equal  $i f_{1;1} G_{1;1}^R$ . However,  $\langle_{1;1}^B$  is a self-energy of the "device" consisting of matrix elements of atom 1 which is not in equilibrium. Therefore, we are not convinced of the validity of this argument even though it does give the correct answer.

$G^<$  is obtained from the Dyson equation for  $G^<$  which, in turn, is obtained from the Dyson equation for the contour ordered Green function by applying the rules of Langreth [71, 109]. The general form is

$$G^< = g^< + g^R G^R G^< + g^R \langle^B G^A + g^< G^A G^A \quad (107)$$

For a single electron perturbation,  $H^0$ , the Dyson equation for the contour ordered Green function is [150]

$$G^P(s; s^0) = g^P(s; s^0) + \int_c^Z ds_1 \int_c^Z ds_2 g^P(s; s_1) H^0(s_1, s_2) G^P(s_2; s^0) \quad (108)$$

where the integrals are along the Keldysh contour [2, 109]. Since the perturbing potential  $H^0$  is local in time,  $\delta(s_1 - s_2)$ ,  $s_1$  and  $s_2$  are always on the same side of the Keldysh contour resulting in the equation for  $G^R$  and  $G^<$  being, respectively [71, 109],

$$G^R(t; t^0) = g^R(t; t^0) + \int_{t_1}^Z dt_2 \int_{t_2}^Z dt_1 g^R(t; t_1) H^0(t_1, t_2) G^R(t_2; t^0) \quad (109)$$

and

$$\begin{aligned} G^<(t; t^0) &= g^<(t; t^0) \\ &+ \int_{t_1}^Z dt_2 \int_{t_2}^Z dt_1 g^R(t; t_1) H^0(t_1, t_2) G^<(t_2; t^0) \\ &+ \int_{t_1}^Z dt_2 \int_{t_2}^Z dt_1 g^<(t; t_1) H^0(t_1, t_2) G^A(t_2; t^0): \end{aligned} \quad (110)$$

In Eq. (110), the term in Eq. (107) containing the self-energy  $\langle^B$  is missing because the local time dependence of the potential forces  $s_1$  and  $s_2$  in (108) to always reside on the same branch of the contour. We now want to check that our new energy-dependent effective potential  $\tilde{\epsilon} = (\tilde{\epsilon} - ES)$  is still local in time and that it does not introduce any memory effects which could give rise to a new term in the usual Dyson equation for  $G^<$ . To check that  $\tilde{\epsilon} = (\tilde{\epsilon} - ES)$ , is still local in time, we need to consider Eqs. (98 - 100) in the time domain. Writing down Eq. (99) in the time domain gives

$$\begin{aligned} G_{0;j}^R(t; t^0) &= \int_{t_1}^Z dt_2 \int_{t_2}^Z dt_1 g_{0;0}^R(t; t_1) \delta_{0;1} + i S_{0;1} \frac{\partial}{\partial t_2} (t_1 - t_2) G_{1;j}^R(t_2; t^0): \end{aligned} \quad (111)$$

Looking at the effective potential in the brackets, it is still local in time. Or, generalizing this to the Keldysh contour,  $t_1$  and  $t_2$  could never be on opposite branches of the contour. Therefore, it appears reasonable that no new self-energy terms are introduced by the effective potential  $\tilde{\epsilon}$  and that by replacing  $t$  with  $\tilde{\epsilon}$ ,  $G^<$  and  $\langle^B$  can be derived from the usual Dyson equations for  $G^<$  as described in detail in ref. [1].

Briefly, for completeness, we write down the Dyson equations for  $G^<$  including only the coupling to the left contact since the equations to include coupling to the right contact are identical in form and can be obtained by replacing subscript 1 with  $N$  and subscript 0 with  $N + 1$ . For any atom  $i; j \in \{1, \dots, N\}$  in the device,

$$G_{i;j}^< = g_{i;j}^< + g_{i;1}^R \tilde{\epsilon}_{1;0} G_{0;j}^< + g_{i;1}^< \tilde{\epsilon}_{1;0} G_{0;j}^A: \quad (112)$$

The Dyson equations for the exact  $G_{0;j}^<$  and  $G_{0;j}^A$  which cross the device-contact boundary are

$$G_{0;j}^< = g_{0;0}^R t_{0;1} G_{1;j}^< + g_{0;0}^< t_{0;1} G_{1;j}^A \quad (113)$$

and

$$G_{0;j}^A = g_{0;0}^A t_{0;1} G_{1;j}^A \quad (114)$$

Substituting Eqs. (114) and (113) back into Eq. (112), gives the exact expression for  $G^<$  of the device.

$$G_{i;j}^< = g_{i;j}^< + g_{i;1}^R \underbrace{t_{1;0} g_{0;0}^R t_{0;1}}_{\substack{R \\ 1;1}} G_{1;j}^< + g_{i;1}^R \underbrace{t_{1;0} g_{0;0}^< t_{0;1}}_{\substack{< \\ 1;1}} G_{1;j}^A + g_{i;1}^< \underbrace{t_{1;0} g_{0;0}^A t_{0;1}}_{\substack{A \\ 1;1}} G_{1;j}^A \quad (115)$$

Multiplying Eq. (115) by the  $N \times N$  block matrix of the isolated device,  $[E S_0 \ H_0] = g^R$ , and using  $[E S_0 \ H_0] g^< = 0$ , we obtain the equation of motion for the contravariant correlation function  $G^<$  in the device domain  $i; j \in \{1, \dots, N\}$ .

$$[E S_0 \ H_0] \ G^< = \ G^< \ G^A \quad (116)$$

$\ G^<$  is obtained from  $\ G^R$ , Eqs. (102) and (103), by replacing  $g^R$  with  $g^<$ , i.e.

$$\ G^< = (t_{1;0} \ E S_{1;0}) g_{0;0}^< (t_{0;1} \ E S_{0;1}) \quad (117)$$

$$\ G^< = (t_{N+1;0} \ E S_{N+1;0}) g_{N+1;N+1}^< (t_{N+1;N} \ E S_{N+1;N}) \quad (118)$$

The one question left is what is  $g_{0;0}^<(E)$  where for any 2 orbitals  $i; j$  associated with atom 0,  $g_{i_0; j_0}^<(E) = i \hbar b_{j_0}^Y b_{i_0}(E) i$ ? Previously, in an orthonormal basis, we say that  $b_{j_0}^Y$  creates the state  $|j_0\rangle$  localized in the left contact which is in equilibrium by definition. Therefore,  $g_{0;0}^<(E)$  is simply the spectral function times the Fermi factor,

$$g_{0;0}^<(E) = i f(E) a_{0;0}(E) \quad (119)$$

where the spectral function  $a = i g^R g^Y$ , and  $f(E)$  is the Fermi factor for an electrochemical potential of the left contact  $\mu_L$ . Now, however,  $b_{j_0}^Y$  creates the state

$$|j_0\rangle = \sum_n \sum_i S_{j_0; i_n}^{-1} |j_{i_n}\rangle \quad (120)$$

which is extended. However,  $g_{0;0}^<(E)$  is the noninteracting correlation function for which there is no overlap between the contact and device states, specially, in our example,  $S_{0;1} = S_{1;0} = 0$ . Therefore,  $S^{-1}$  is block diagonal with no matrix elements coupling the contacts to the device and the sum in (120) is nonzero only for atoms  $n$  in the left contact,  $n \in \{1, \dots, 0\}$ . Therefore, for the noninteracting  $g_{0;0}^<$ ,  $b_{j_0}^Y$  and  $b_{i_0}$  only create and annihilate states in the left contact which is in equilibrium so that (119) still holds. The equations for the correlation function  $G^<$  and Green function  $G^R$  are now formally identical to those derived previously for orthogonal basis sets [1].

## D. Current

### 1. Standard Expression

The derivation of the current operator generally starts with an expression for the local electron density which is then placed into the continuity equation to give an expression for the local divergence of the current [71]. Instead of a local continuity equation, we will write a continuity equation for the total number of electrons contained in the orbitals that are elements of the "device." Note that we are defining the "device" as a set of orbitals rather than a region of space. The total electron number is

$$\begin{aligned} N_D &= \sum_{a \neq b} \sum_{i_a; j_b} \sum_{i_a} G_{i_a; j_b}^<(t; t) \int d^3 r \delta_{j_b}(r) \delta_{i_a}(r) \\ &= i \text{tr} S_0 G^<(t; t) \end{aligned} \quad (121)$$

where  $a$  and  $b$  index the atoms in the "device,"  $i_a$  indexes an orbital of atom  $a$ , and the trace is over all states in the "device." We now take the time derivative of  $N_D$  as

$$\frac{\partial N_D}{\partial t} = i \text{tr} S_0 \lim_{t \rightarrow t^0} \left( \frac{\partial}{\partial t} + \frac{\partial}{\partial t^0} \right) G^<(t; t^0) \quad (122)$$

The equation of motion for  $G^<(t; t^0)$  in the device is

$$i \frac{\partial}{\partial t} S_0 G^<(t; t^0) - H_0 G^<(t; t^0) = \int dt_1 \left[ G^<(t; t_1) G^<(t_1; t^0) + G^<(t; t_1) G^A(t_1; t^0) \right] \quad (123)$$

and the conjugate equation is [6]

$$i \frac{\partial}{\partial t^0} G^<(t; t^0) S_0 - G^<(t; t^0) H_0 = \int dt_1 \left[ G^<(t; t_1) G^A(t_1; t^0) + G^R(t; t_1) G^<(t_1; t^0) \right] \quad (124)$$

Subtracting Eq. (123) from Eq. (124), taking the limit  $t \rightarrow t^0$ , and the tracing over all device states, we have

$$\begin{aligned} \frac{\partial N_D}{\partial t} + \text{tr} \int dt_1 \left[ G^<(t; t_1) G^<(t_1; t) H_0 - G^<(t; t_1) G^A(t_1; t) \right. \\ \left. - G^R(t; t_1) G^<(t_1; t) + G^<(t; t_1) G^A(t_1; t) \right] = 0 \end{aligned} \quad (125)$$

Eq. (125) is the continuity equation for the total electron number within the orbitals that define the "device." In steady-state,  $\frac{\partial N_D}{\partial t} = 0$ . The second term is also 0 due to the cyclic invariance of the trace. The last term must also be zero, but we can break it up into contributions from the left and right contacts. These contributions will be equal in magnitude and opposite in sign. For our linear chain nearest neighbor example, the self-energies resulting from coupling of the device to the left contact are non-zero only for the orbitals of atom 1. Similarly, the self-energies resulting from coupling of the device to the right contact are only non-zero for the orbitals of atom  $N$ .

Fourier transforming the last term of Eq. (125), the particle current flowing out of the left contact into the device is

$$J = \int \frac{dE}{2\pi} \text{tr} \int dt_1 \left[ G^<(E) G^A(E) + G^R(E) G^<(E) - G^R(E) G^<(E) - G^A(E) G^<(E) \right] \quad (126)$$

where the trace is over the orbitals of atom 1. We regroup terms using the cyclic invariance of the trace to obtain

$$\begin{aligned} J &= \int \frac{dE}{2\pi} \text{tr} \left[ G^<(E) G^R(E) - G^A(E) G^<(E) \right] \\ &= \int \frac{dE}{2\pi} \text{tr} \left[ f_L A_{1,1} + i G^<(E) \right] \end{aligned} \quad (127)$$

This current expression was first written down by Meir and Wingreen [148]. In Eq. (127),  $f_L$  is the Fermi factor of the left contact,  $B_{1,1} = i G^R_{1,1} G^A_{1,1}$ , and  $A_{1,1} = i G^R_{1,1} G^A_{1,1}$  where, for example,  $G^R_{1,1}$  is the sub-block matrix of  $G^R$  consisting of orbitals of atom 1.

The integrand of Eq. (127) satisfies the following equality [1, 148]

$$B_{1,1} f_L A_{1,1} + i G^<(E) = \tau_{0,1} G^<(E) - \tau_{1,0} G^<(E) \quad (128)$$

This is derived by inserting the Dyson equations for  $G^<(E)$  and  $G^<(E)$

$$G^<(E) = g_{0,0}^R \tau_{0,1} G^<(E) + g_{0,0}^< \tau_{0,1} G^A_{1,1} \quad (129)$$

$$G^<(E) = G^R_{1,1} \tau_{1,0} g_{0,0}^< + G^<(E) \tau_{1,0} g_{0,0}^A \quad (130)$$

into the right hand side of Eq. (128). Therefore, the general expression for the current Eq. (127) is also given by

$$J = \frac{Z}{2} \frac{dE}{\sim} \text{tr} \left( t_{0;1} G_{1;0}^< \quad t_{1;0} G_{0;1}^< \right) \quad (131)$$

Since there is nothing special about atoms 0 and 1, we can say that Eq. (127) implies that the current flowing between any 2 atoms  $n$  and  $n+1$  in the chain is

$$J = \frac{Z}{2} \frac{dE}{\sim} \text{tr} \left( t_{n;n+1} G_{n+1;n}^< \quad t_{n+1;n} G_{n;n+1}^< \right) \quad (132)$$

or explicitly writing out the  $t$  terms,

$$J = \frac{Z}{2} \frac{dE}{\sim} \text{tr} \left( (t_{n;n+1} - E S_{n;n+1}) G_{n+1;n}^< \quad (t_{n+1;n} - E S_{n+1;n}) G_{n;n+1}^< \right) \quad (133)$$

Eqs. (131), (132) and (133) are identical to those obtained from empirical tight binding models [1, 71].

The matrix elements  $(t - E S)_{\sim}$  can be thought of as a transition rate coupling orbitals from atoms  $n$  and  $n+1$ . It is not immediately clear that  $E S$  should enter into the dynamics. We will show below that these are the correct matrix elements which result in unitary transition probabilities for a band of a periodic system.

For coherent transport,  $G^< = G^R <^B G^A$  and  $A = G^R >^B G^A$  or writing out these expressions explicitly,

$$G_{1;1}^< = G_{1;1}^R \text{if}_L^B G_{1;1}^A + G_{1;N}^R \text{if}_R^B G_{N;1}^A \quad (134)$$

and

$$A_{1;1} = G_{1;1}^R \text{if}_L^B G_{1;1}^A + G_{1;N}^R \text{if}_R^B G_{N;1}^A \quad (135)$$

Inserting the above two equations into Eq. (127) results in the usual form for the coherent current [1, 119, 148].

$$J = \frac{Z}{2} \frac{dE}{\sim} \text{tr} \left( t_{1;1} G_{1;N}^R \text{if}_R^B G_{N;1}^A \quad (f_L - f_R) \right) \quad (136)$$

This equation was first derived by Caroli et al. [71] (see their Eq. (42)) and then later by Fisher and Lee [119] and then many others [148].

Once one has derived an expression for the transmission coefficient, it is always wise to check that for a periodic, uniform system, the transmission is 1.0 independent of energy within a propagating band. We will now perform this check of Eq. (136) for a linear chain of atoms with one orbital per atom. The Hamiltonian matrix elements are  $\langle n | H | j_n \rangle = t$  and  $\langle n | H | j_{n-1} \rangle = t$  where  $n$  is the atom index. The overlaps are  $\langle n | j_{n-1} \rangle = s$  and  $\langle n | j_n \rangle = 1$ . Applying the Hamiltonian to the ansatz  $| j_i \rangle = \sum_n | j_n \rangle z^n$  results in

$$E = (t - E s) z^{-1} + t + (t - E s) z \quad (137)$$

Substituting the phase factor  $z = e^{ik}$  into (137) results in the  $E - k$  dispersion relation

$$E - t + 2(t - E s) \cos(k) = 0 \quad (138)$$

Since we are considering a uniform infinite chain of atoms, our device will consist of 1 atom,  $n = 1$ . The surface Green function  $g_s^R = g_{0;0}^R = g_{2;2}^R$  of both the left and right leads is given by the recursion relation

$$g_s^R = E - (t - E s) g_s^R (t - E s)^{-1} \quad (139)$$

Eq. (139) simply states that the surface Green function of the semi-infinite chain ending at site 0 is the same as the surface Green function of the semi-infinite chain ending at site -1. Eq. (137) is a quadratic equation for  $z$  and Eq. (139) is a quadratic equation for  $g_s^R$ . Writing out the solution for both equations, one finds that

$$g_s^R = \frac{z}{t - E s} = \frac{e^{ik}}{t - E s} = \frac{\cos(k) + i \sin(k)}{t - E s} \quad (140)$$

The boundary self-energy for both the left and right contact is

$$\Gamma^R = (t - E s) g_s^R (t - E s) \quad (141)$$

and

$$\Gamma^B = \Gamma^L = \Gamma^R = 2\text{Im} \Gamma^B = 2(t - E s) \sin(k) \quad (142)$$

The superscripts L and R indicate that the quantity is the result of coupling to the left or right contact, respectively. The exact Green function on site 1 is

$$\begin{aligned} G_{1;1}^R &= E - 2(t - E s) \Gamma^R (t - E s)^{-1} \\ &= [E - 2(t - E s) (\cos(k) + i \sin(k))]^{-1} \\ &= [2i(t - E s) \sin(k)]^{-1} \\ &= \frac{1}{i \frac{1}{2} (\Gamma^L + \Gamma^R)} = \frac{1}{i \Gamma^B} \end{aligned} \quad (143)$$

The factor of 2 comes from the two identical self energies from the left and right leads. In the second to last line, the real part is zero from the dispersion relation Eq. (138). The transmission coefficient from Eq. (136) is  $T = \frac{\Gamma^L}{1;1} G_{1;1}^R \frac{\Gamma^R}{1;1} G_{1;1}^R$  which, for scalar quantities, is

$$T = \frac{\Gamma^B}{\Gamma^B} G_{1;1}^R{}^2 \quad (144)$$

where  $\Gamma^B = \Gamma^L = \Gamma^R$ . Substituting Eq. (143) into Eq. (144) results in a unitary transmission probability.

$$T = \frac{\Gamma^B}{\Gamma^B} = 1 \quad (145)$$

This demonstrates that the matrix elements  $t - E s$  are the correct ones to use in the current equations.

With these expressions for the current Eqs. (127), (131), (133), and (136), we have re-derived NEGF theory for a non-orthogonal basis that is formally identical to that for an orthogonal basis. The equations for the correlation function  $G^<$ , the Green function  $G^R$ , and the current  $J$ , are now formally identical and can be obtained by simply replacing the off-diagonal Hamiltonian matrix elements  $t$  with  $t - E s$ . All of the efficient numerical algorithms developed previously, such as the current expressions and recursive Green function algorithms, can be applied [1, 29, 30].

## 2. Direct Evaluation of Current Operator

In deriving the standard current equation (127), we started by calculating the current flowing out a specific set of orbitals rather than a region of space. Since our model has a specific basis, it would appear that we do not need to make this approximation, and we can directly calculate the surface integral of the current crossing a plane. However, we will demonstrate by example that for an incomplete basis such a straightforward calculation results in an expression for the current which violates particle conservation and does not reduce to unitary transmission for coherent transport within a band.

For evaluating the surface integral of the current crossing a plane, we choose the plane between the atoms 0 and 1, i.e. between the left contact and the device. The expectation value of the current crossing the plane is

$$\langle J \rangle = \int_{\mathcal{Z}} ds \langle J(x) \rangle = \frac{i\hbar}{2m} \int_{\mathcal{Z}} ds \langle \psi^y(x) \psi^x(x) - \psi^y(x) \psi^x(x) \rangle \quad (146)$$

$$= \frac{i\hbar}{2m} \int_{\mathcal{Z}} ds \lim_{r^0 \rightarrow r} \langle \psi^y(x) \psi^x(x) G^<(x;t;r^0;t) \rangle \quad (147)$$

$$\begin{aligned} &= \frac{i\hbar}{2m} \int_{\mathcal{Z}} ds \langle \psi_j^y(x) \psi_i^x(x) \rangle \langle \psi_j(x) \psi_i(x) \rangle \\ &= \frac{i\hbar}{2m} \int_{\mathcal{Z}} ds \langle \psi_j^y(x) \psi_i^x(x) \rangle \langle \psi_j(x) \psi_i(x) \rangle \end{aligned} \quad (148)$$

Eq. (148) is the one that we will use. We write it in the form of Eq. (147) to show that for a complete basis, the value of the surface integral is independent of position along the wire.

We take the plane of integration to be the  $xy$  plane. Fourier transforming into the energy domain and taking  $\partial = \partial_z$  of Eq. (147) results in

$$\frac{\partial}{\partial z} J = \frac{\tilde{r}^2}{2m} \int \frac{dE}{2} \int dx \int dy \lim_{r^0 \rightarrow r} \frac{\partial^2}{\partial z^2} \frac{\partial^2}{\partial z^2} G^<(r; r^0; E) \quad (149)$$

Using the equations of motion for  $G^<(r; r^0; E)$  within the device

$$E + \frac{\tilde{r}^2 r^2}{2m} V(r) G^<(r; r^0; E) = 0 \quad (150)$$

$$E + \frac{\tilde{r}^2 r^2}{2m} V(r^0) G^<(r; r^0; E) = 0 \quad (151)$$

Eq. (149) becomes

$$\frac{\partial}{\partial z} J = \frac{\tilde{r}^2}{2m} \int \frac{dE}{2} \int dx \int dy \lim_{r^0 \rightarrow r} \frac{\partial^2}{\partial x^2} + \frac{\partial^2}{\partial y^2} \frac{\partial^2}{\partial x^2} \frac{\partial^2}{\partial y^2} G^<(r; r^0; E) \quad (152)$$

Integrating by parts using

$$\frac{\partial}{\partial x} G^<(r; r^0; E) = \lim_{r^0 \rightarrow r} \frac{\partial}{\partial x} + \frac{\partial}{\partial x^0} G^<(r; r^0; E) \quad (153)$$

Eq. (152) is equal to zero. This is perhaps easier to see by re-writing Eq. (152) back in the form of Eq. (146).

We now return to Eq. (148) which we write out explicitly as

$$J = \sum_{i,j} G^<_{i,j}(t;t) \int dx \int dy \frac{\tilde{r}^2}{2m} j(r) \frac{\partial}{\partial z} \psi_i(r) \psi_j(r) \frac{\partial}{\partial z} \psi_j(r) \quad (154)$$

We evaluate (154) at  $z$  between sites 0 and 1. The only nonzero contributions come from the orbitals that cut the surface between atoms 0 and 1. In our nearest neighbor example, only the orbitals of atoms 0 and 1 contribute to the integral. The integral in (154) contains 4 terms, 2 intra-atomic terms and 2 inter-atomic terms. We will first consider the inter-atomic terms since these 2 terms will result in an expression formally identical to Eq. (131) but with different matrix elements.

The inter-atomic terms are

$$J_t = \sum_{i_0, j_1} M_{i_0, j_1} M_{j_1, i_0} G^<_{j_1, i_0}(t;t) + M_{j_1, i_0} M_{i_0, j_1} G^<_{i_0, j_1}(t;t) \quad (155)$$

where  $M_{i,j}$  is the matrix element  $\int dx \int dy \frac{\tilde{r}^2}{2m} \psi_i(r) \frac{\partial}{\partial z} \psi_j(r)$ .

We define the current matrix element as

$$J_{i_0, j_1} = M_{i_0, j_1} M_{j_1, i_0} \quad (156)$$

and Eq. (155) becomes

$$\begin{aligned} J_t &= \sum_{i_0, j_1} J_{i_0, j_1} G^<_{j_1, i_0}(t;t) + J_{j_1, i_0} G^<_{i_0, j_1}(t;t) \\ &= \text{tr} \sum_n J_{0,1} G^<_{1,0}(t;t) + J_{1,0} G^<_{0,1}(t;t) \\ &= \frac{dE}{2} \text{tr} \sum_n J_{0,1} G^<_{1,0}(E) J_{0,1}^y G^<_{0,1}(E) \end{aligned} \quad (157)$$

where in the last line we used  $J_{0,1}^y = J_{1,0}$ .

Eq. (157) is a general expression for the current. We can move the plane to cut between any two atoms of the chain, so that we have an expression for calculating the current at any point in the device. For example, cutting between atoms  $n$  and  $n+1$ , the current would be

$$J_t = \frac{dE}{2} \text{tr} \sum_n J_{n, n+1} G^<_{n+1, n}(E) J_{n, n+1}^y G^<_{n, n+1}(E) \quad (158)$$

From now on, we will work in the energy domain and save on notation by defining  $J_t(E)$  as  $J_t(E) = \text{tr} J_{0;1} G_{1;0}^<(E) J_{0;1}^y G_{0;1}^<(E)$ . We will also use the matrix notation of the last line of Eq. (157). The bold quantities indicate matrices the size of the localized orbital basis per atom and the subscripts indicate from which atom the orbitals come. The trace is over the orbitals equivalent to the  $i_0, j_1$  in Eq. (157).

To bring Eq. (157) into a form comparable to Eq. (127) or Eq. (136), we begin by substituting the Dyson Equations for  $G_{0;1}^<$  and  $G_{1;0}^<$  Eqs. (129) and (130) into Eq. (157) to obtain

$$J_t(E) = \text{tr} \begin{matrix} n \\ J_{0;1} G_{1;1}^R \boldsymbol{\epsilon}_{1;0} G_{0;0}^< + J_{0;1} G_{1;1}^< \boldsymbol{\epsilon}_{1;0} g_{0;0}^A \end{matrix} \begin{matrix} J_{0;1}^y g_{0;0}^R \boldsymbol{\epsilon}_{0;1} G_{1;1}^< \\ J_{0;1}^y g_{0;0}^< \boldsymbol{\epsilon}_{0;1} G_{1;1}^A \end{matrix} \begin{matrix} o \\ \end{matrix} : \quad (159)$$

Eq. (159) is the equivalent of Eq. (127). If the Js were replaced by  $\boldsymbol{\epsilon}$ s, then Eq. (159) would be identical to Eq. (127). Grouping the terms of Eq. (159) with  $G_{1;1}^<$  together and using the cyclic invariance of the trace, Eq. (159) becomes

$$\begin{aligned} J_t(E) &= \text{tr} \begin{matrix} i \\ J_{0;1}^y g_{0;0}^R \boldsymbol{\epsilon}_{0;1} \end{matrix} \begin{matrix} J_{0;1}^y g_{0;0}^R \boldsymbol{\epsilon}_{0;1} \end{matrix} \begin{matrix} y \\ i G_{1;1}^< \end{matrix} \\ &\quad + \text{tr} \begin{matrix} n \\ \boldsymbol{\epsilon}_{1;0} g_{0;0}^< J_{0;1} G_{1;1}^R \end{matrix} \begin{matrix} J_{0;1}^y g_{0;0}^< \boldsymbol{\epsilon}_{1;0} G_{1;1}^A \end{matrix} \begin{matrix} o \\ \end{matrix} \\ &= \text{tr} \begin{matrix} J \\ 1;1 \end{matrix} i G_{1;1}^< + \text{tr} \begin{matrix} n \\ \boldsymbol{\epsilon}_{1;0} g_{0;0}^< J_{0;1} G_{1;1}^R \end{matrix} \begin{matrix} J_{0;1}^y g_{0;0}^< \boldsymbol{\epsilon}_{1;0} G_{1;1}^A \end{matrix} \begin{matrix} o \\ \end{matrix} \end{aligned} \quad (160)$$

where we used  $\boldsymbol{\epsilon}_{0;1}^y = \boldsymbol{\epsilon}_{1;0}$ ,  $g_{0;0}^R J^y = g_{0;0}^A$ , and defined

$$\begin{matrix} J \\ 1;1 \end{matrix} \equiv i \begin{matrix} J_{0;1}^y g_{0;0}^R \boldsymbol{\epsilon}_{0;1} \\ J_{0;1}^y g_{0;0}^R \boldsymbol{\epsilon}_{0;1} \end{matrix} \begin{matrix} y \\ \end{matrix} : \quad (161)$$

Eq. (160) is exact, valid with or without incoherent processes in the device.

The 2 intra-atomic terms from Eq. (154) result in a current term

$$J_a = \frac{Z}{2} \frac{dE}{\sim} \text{tr} \begin{matrix} J_{0;0} G_{0;0}^<(E) \\ J_{1;1} G_{1;1}^<(E) \end{matrix} \quad (162)$$

In equilibrium when  $G^< = i f_A$ , the intra-atomic terms are individually 0 since for our real orbitals,  $A(t;t) = S^{-1}$  is symmetric and  $J$  is antisymmetric.  $G_{0;0}^<(E)$  is the exact  $G^<$  in the left contact, which is, since the contact is by definition in equilibrium,  $G_{0;0}^<(E) = i f_L A_{0;0}(E)$  [151]. Therefore, the first term of Eq. (162) is always zero for a basis of real orbitals.

For coherent transport, we can bring the sum of Eqs. (160) and Eq. (162) into the Fisher-Lee form for the transmission coefficient. Substituting [151]

$$G_{1;1}^< = i f_L G_{1;1}^R \begin{matrix} B \\ 1;1 \end{matrix} G_{1;1}^A + i f_R G_{1;1}^R \begin{matrix} B \\ N;N \end{matrix} G_{N;1}^A \quad (163)$$

into Eq. (160) gives

$$\begin{aligned} J_t(E) &= \text{tr} f \begin{matrix} J \\ 1;1 \end{matrix} G_{1;1}^R \begin{matrix} B \\ N;N \end{matrix} G_{N;1}^A g f_R \\ &\quad + \text{tr} \begin{matrix} J \\ 1;1 \end{matrix} G_{1;1}^R \begin{matrix} B \\ 1;1 \end{matrix} G_{1;1}^A + i \boldsymbol{\epsilon}_{1;0} a_{0;0} J_{0;1} G_{1;1}^R \begin{matrix} J_{0;1}^y a_{0;0} \boldsymbol{\epsilon}_{0;1} G_{1;1}^A \\ f_L \end{matrix} \end{aligned} \quad (164)$$

where in the second line we used the relation  $g_{0;0}^< = i f_L a_{0;0}$ . Substituting Eq. (163) into the intra-atomic current term Eq. (162) gives [151]

$$J_a = \frac{Z}{2} \frac{dE}{\sim} \text{tr} \begin{matrix} i f_L J_{1;1} G_{1;1}^R \begin{matrix} B \\ 1;1 \end{matrix} G_{1;1}^A \\ i f_R J_{1;1} G_{1;1}^R \begin{matrix} B \\ N;N \end{matrix} G_{N;1}^A \end{matrix} \quad (165)$$

The total coherent current is the sum of the intra-atomic Eq. (165) and inter-atomic Eq. (164) contributions.

In equilibrium, when  $f_L = f_R$ , the current must be 0. Furthermore, we can, in principle change  $f_L$  and  $f_R$  independently of the transmission coefficient. Therefore, the term proportional to  $f_L$  must be equal in magnitude and opposite in sign to the term proportional to  $f_R$ . Both terms are alternative expressions for the transmission coefficient. The term proportional to  $f_R$  is in the standard Fisher-Lee form so that we can write

$$J = \frac{Z}{2} \frac{dE}{\sim} \text{tr} \begin{matrix} J_{1;1} \\ i J_{1;1} G_{1;1}^R \begin{matrix} B \\ N;N \end{matrix} G_{N;1}^A \end{matrix} (f_L - f_R) \quad (166)$$



We note that the other term of Eq. (164) is the more computationally efficient form equivalent to Eq. (53) of ref. [1]. Also,  $J_{1;1}^J$  is Hermitian and the product  $G_{1;N}^R \mathbb{B}_{N;N} G_{N;1}^A$  is Hermitian. Therefore, the trace  $\text{tr} J_{1;1}^J G_{1;N}^R \mathbb{B}_{N;N} G_{N;1}^A$  is real. Conversely,  $J_{1;1}$  is antisymmetric so that  $i \text{tr} J_{1;1} G_{1;N}^R \mathbb{B}_{N;N} G_{N;1}^A$  is also real. Eq. (166) is identical to the expression that is universally used [37, 48, 51, 52, 54, 74] Eq. (136) with the replacement of  $J_{1;1}$  with  $(J_{1;1}^J - iJ_{1;1})$ .

With current expression (166) we investigate the consequence of an incomplete basis by evaluating the value of the transmission probability for a periodic, uniform system as we did for the "standard" current expression Eq. (136). Using the same single-band model described immediately preceding Eq. (137), the intra-atomic term  $J_{1;1}$  is 0. The factor  $J^J$  is

$$J^J = 2 \text{Im} J_{0;1} g_s^R(t, E_s) = 2J_{0;1} \sin(k) \quad (167)$$

The transmission coefficient Eq. (166) is then

$$T = \frac{J_{0;1}^J}{t(E_s)} \quad (168)$$

The transmission probability of Eq. (168) can only equal unity if  $J_{0;1} = t(E_s)$ . Since  $t(E_s)$  is energy dependent, this is clearly not possible. Therefore, this "exact" evaluation of the current leads to qualitatively incorrect results for an incomplete basis. With an incomplete basis, one should derive the current expression from conservation laws that are consistent with the Hamiltonian and basis such as Eqs. (121) – (125). We note the strong parallel here with the discussions in the literature concerning the form of the momentum matrix element in empirical tight binding theory in which the explicit basis is not known [108, 152, 153, 154].

### 3. Equivalence of the Standard and Exact Current Expressions in a Complete Basis

The argument for the equivalence of the two current expressions, Eqs. (127) or (131) and Eqs. (157) plus (162) is based on particle conservation by writing the current as the time derivative of the electron number in the left contact [155]. For lack of better expressions we will refer to the current in the "standard" expressions Eqs. (127) or (131) as the "tight-binding current" ( $J_{\text{tb}}$ ). We will refer to the current derived from the direct evaluation of the current operator Eq. (147) as the "real space current" ( $J_z$ ).

For the real space current, Eq. (147) is derived from the continuity equation, and it is equal to the negative time derivative of the electron number in the left contact (for the surface chosen between atoms 0 and 1). It is given by

$$\begin{aligned} J_z &= \frac{\partial N_z^L}{\partial t} = \frac{\partial}{\partial t} \int_{-Z}^Z dx \int_{-Z}^Z dy \int_{z_0}^Z dz h^y(x, y, z) \\ &= i \int_{i,j} \frac{\partial}{\partial t} G_{i,j}^<(t;t) dx dy dz j(x) i(x) \end{aligned} \quad (169)$$

where  $N_z^L$  is the electron number of the left contact and  $z_0$  lies between atoms 0 and 1.

The tight binding current Eqs. (127) or (131) were derived by considering the time derivative of the electron number of the orbitals in the "device." It can also be derived by considering the time derivative of the electron number of the orbitals in the left lead. Although this seems physically obvious, it is not straightforward to show, therefore below, we write down the main steps.

The electron number in the left contact is given by the sum over all of the orbitals of the left contact,

$$\begin{aligned} N_{\text{tb}}^L &= i \sum_{a;b=1}^X \sum_{i_a;j_b}^X G_{i_a;j_b}^<(t;t) \int_{-Z}^Z d^3r j_b(x) i_a(x) \\ &= i \text{tr} S_0 G^<(t;t) \end{aligned} \quad (170)$$

where the trace is over all orbitals of the left contact. We need an equation for the exact  $G^<$  of the left contact in terms of the exact Green functions of the device. Minding the steps used to derive  $G^<$  of the device Eqs. (112) – (116) we write the Dyson equations for the left contact. For any atom  $s; j \in \{1, 2, \dots, 0\}$  in the left contact,

$$G_{i;j}^< = g_{i;j}^< + g_{i;0}^R \mathbb{t}_{0;1} G_{1;j}^< + g_{i;0}^< \mathbb{t}_{0;1} G_{1;j}^A \quad (171)$$

The Dyson equations for the exact  $G_{1;j}^<$  and  $G_{1;j}^A$  which cross the device-contact boundary are

$$G_{1;j}^< = G_{1;1}^R \mathbb{t}_{1;0} G_{0;j}^< + G_{1;1}^< \mathbb{t}_{1;0} G_{0;j}^A \quad (172)$$

and

$$G_{1,j}^A = G_{1,1}^A \tau_{1,0}^A g_{0,j}^A \quad (173)$$

Substituting Eqs. (173) and (172) back into Eq. (171), gives the exact expression for  $G^<$  of the left lead.

$$G_{i,j}^< = g_{i,j}^< + g_{i,0}^R \tau_{0,1}^R G_{1,1}^R \tau_{1,0}^R g_{0,j}^< + g_{i,0}^R \tau_{0,1}^R G_{1,1}^< \tau_{1,0}^R g_{0,j}^A + g_{i,0}^< \tau_{0,1}^< G_{1,1}^A \tau_{1,0}^A g_{0,j}^A \quad (174)$$

Multiplying (174) on the left with  $g^{R-1} = [S_0 \ H_0]$  results in

$$\sum_{k=1}^{X^0} [S_0 \ H_0]_{i,k} G_{k,j}^< = \sum_{0,0}^{\substack{R \\ B}} \tau_{0,1}^R G_{1,1}^R \tau_{1,0}^R g_{0,j}^< + \sum_{0,0}^{\substack{< \\ B}} \tau_{0,1}^< G_{1,1}^< \tau_{1,0}^< g_{0,j}^A : \quad (175)$$

In the time domain we have

$$i \sim \frac{\partial}{\partial t} S_0 G^<(t; t^0) \ H_0 G^<(t; t^0) = \int dt_1 \ \tau^{RB}(t; t_1) g^<(t_1; t^0) + \int dt_1 \ \tau^{<B}(t; t_1) g^A(t_1; t^0) \quad (176)$$

and

$$i \sim \frac{\partial}{\partial t^0} G^<(t; t^0) S_0 \ G^<(t; t^0) H_0 = \int dt_1 \ g^<(t; t_1) \ \tau^{AB}(t_1; t^0) + \int dt_1 \ g^R(t; t_1) \ \tau^{<B}(t_1; t^0) \quad (177)$$

Subtracting Eq. (176) from Eq. (177), taking the limit  $t^0 \rightarrow t$ , and the tracing over all contact states, we have

$$\begin{aligned} \frac{\partial N_{tb}^L}{\partial t} + \text{tr} \int dt_1 \ H_0 G^<(t; t_1) \ G^<(t; t_1) H_0 \\ - \int dt_1 \ \text{tr} f g^<(t; t_1) \ \tau^{AB}(t_1; t) + g^R(t; t_1) \ \tau^{<B}(t_1; t) \\ - \int dt_1 \ \tau^{RB}(t; t_1) g^<(t_1; t) \ - \int dt_1 \ \tau^{<B}(t; t_1) g^A(t_1; t) g = 0 : \end{aligned} \quad (178)$$

The second term in Eq. (178) is zero due to the cyclic invariance of the trace. Writing out the last term we get that the current flowing out of the left contact is

$$J_{tb} = \frac{\partial N_{tb}^L}{\partial t} = \int dt_1 \ \text{tr} f \tau_{0,1}^R G_{1,1}^R \tau_{1,0}^R g_{0,0}^< + \tau_{0,1}^< G_{1,1}^< \tau_{1,0}^< g_{0,0}^A - \int dt_1 \ g_{0,0}^< \tau_{0,1}^R G_{1,1}^A \tau_{1,0}^R - \int dt_1 \ g_{0,0}^R \tau_{0,1}^< G_{1,1}^< \tau_{1,0}^< g : \quad (179)$$

Cyclically permuting the terms under the trace, Eq. (179) is identical to Eq. (126) derived by considering the time derivative of the electron number of the device.

Now that we have shown that both currents are equal to the negative time derivative of the total electron number of the left contact, we take the long time average of the current.

$$\langle J_z \rangle = \frac{1}{2} \int dt J_z = \langle N_z^L \rangle - \langle N_z^L \rangle = 2 \quad (180)$$

Similarly

$$\langle J_{tb} \rangle = \frac{1}{2} \int dt J_{tb} = \langle N_{tb}^L \rangle - \langle N_{tb}^L \rangle = 2 \quad (181)$$

The only difference between these two expressions lies in the orbitals near the plane between atoms 0 and 1. The integral defining  $N_z^L$  contains part of the orbitals of atom 0 and part of the orbitals of atom 1. The integral defining  $N_{tb}^L$  contains all of the orbitals of atom 0 and none of the orbitals of atom 1. We can say that the difference between  $\langle J_{tb} \rangle$  and  $\langle J_z \rangle$  must be bounded by

$$\sum_{a,b=0}^{X^1} \sum_{i,j}^X G_{i_a i_b}^<( ; ) - G_{i_a i_b}^<( ; ) = \int d^3 r \ j_b(r) \ i_a(r) = 2 \quad (182)$$

where  $a$  and  $b$  label the atom index and  $i$  and  $j$  are the orbital index. If the quantity within the vertical brackets is finite, then the long time average of the two current expressions must be identical. We note that a rigorous mathematical proof requires careful construction of the scattering states an example of which is given in Appendix A of [156], and also care in taking the appropriate long time limits for both the scattering state and the adiabatic turn on of the device-contact coupling.

To conclude this section, we re-state the fact that the "standard" current expressions are the correct ones since they result in a unitary transmission probability within the band of a periodic system. The "standard" current expressions Eqs. (127) and (132) are identical in form to the current expressions derived for an orthonormal basis. The only difference is that the Hamiltonian matrix element  $t$  is replaced everywhere by the effective Hamiltonian matrix element  $\tilde{t} = t - ES$ .

Even with an explicit basis, one should derive the current expression from conservation laws that are consistent with the Hamiltonian and basis such as Eqs. (121) – (125). A direct evaluation of the real space current operator in an incomplete basis will lead to a breakdown of the particle conservation law and qualitatively incorrect results. For a complete basis, the 2 approaches should give the same result.

## VII. CONCLUSION

In summary, the use of the NEGF approach to quantum electron transport developed in the early 1970s is continuing to increase. So much so that one could argue that it is the most heavily used approach for modeling quantum electron transport through nanostructures ranging from semiconductors to carbon nanotubes to molecules.

Currently, the heaviest usage is in the area of molecular electronics in which the NEGF approach is used to model current-voltage characteristics of molecules. All of the NEGF applications in this area, of which we are aware, model coherent transport through the molecule. The majority of the reported implementations combine DFT with NEGF often integrating the NEGF algorithm with existing ab-initio commercial quantum chemistry or computational materials codes. These codes use an explicit non-orthogonal localized orbital basis. The formulation of the standard NEGF approach to open system boundaries in a non-orthogonal basis raises questions that have not been addressed in the literature.

To address those questions, we have re-derived the standard NEGF theory in a non-orthogonal basis using the second quantized formalism that underlies the theory. This has allowed us to explore some of the approximations that are commonly made, but of which, one finds little discussion. The most fundamental approximation lies in the compatibility of NEGF based on adiabatic perturbation theory and unitary evolution of states with changes in the basis states and corresponding Hilbert space. This issue does not arise if one is only interested in  $G^R$  since NEGF theory is not required to get  $G^R$ . It can be obtained from the Heisenberg equation of motion and matrix algebra as shown by the derivation of Eq. (104). In nonequilibrium, one must obtain  $G^<$  from the contour ordered Dyson equation, which, in principle, does not appear to be compatible with perturbations in the basis states. However, once  $G^{R,B}$  is fixed by the derivation of  $G^R$ , the options for  $G^{<B}$  and thus  $G^<$  become limited, and the standard expression for  $G^{<B}$  Eqs. (117) and (118) found in the literature appears reasonable.

The second approximation underlies the derivation of the "standard" current expression Eq. (127-136). We were unable to find a form for the local electron density from which one could derive these expressions from a local continuity equation. Instead, we wrote a continuity equation for the total number of electrons in a set of orbitals that define the "device" or left contact rather than in a specific region of space. In the coherent limit, the resulting expression for the transmission probability gives the correct unitary value for a periodic system.

A direct evaluation of the real space current operator in an incomplete basis will lead to a breakdown of the particle conservation law and qualitatively incorrect results. For a complete basis, the standard approach and the direct evaluation of the real space current operator should give the same result.

## Acknowledgments

We acknowledge very helpful discussions with A. K. Krotkov. This work was supported by the NSF (DMR-0103248), DOD/DARPA/DMEA (DMEA 90-02-2-0216), and the Microelectronics Advanced Research Corporation Focus Center on Nano Materials.

- 
- [1] R. Lake, G. Klimeck, R. C. Bowen, and D. Jovanovic, *J. Appl. Phys.* 81, 7845 (1997).
- [2] L. V. Keldysh, *Sov. Phys. JETP* 20, 1018 (1965).
- [3] L. P. Kadano and G. Baym, *Quantum Statistical Mechanics* (Adison-Wesley, New York, 1989).
- [4] H. Haug, *Optical Nonlinearities and Instabilities in Semiconductors* (Academic Press, New York, 1988).
- [5] A. P. Jauho and J. W. Wilkins, *Phys. Rev. B* 29, 1919 (1984).
- [6] G. D. Mahan, *Physics Reports* 145, 251 (1987).
- [7] R. Bertoncini and A. P. Jauho, *Phys. Rev. Lett.* 68, 2826 (1992).
- [8] G. Kim and G. B. Arnold, *Phys. Rev. B* 38, 3252 (1988).
- [9] E. V. Anda and F. Flores, *J. Phys.: Condens. Matter* 3, 9087 (1991).
- [10] L. Y. Chen and C. S. Ting, *Phys. Rev. Lett.* 64, 3159 (1990).
- [11] R. K. Lake and S. Datta, *Superlattices and Microstructures* 11, 83 (1992).
- [12] J. Zang and J. L. Bimian, *Phys. Rev. B* 46, 5020 (1992).
- [13] C. H. Rein, E. Runge, and H. Ehrenreich, *Phys. Rev. B* 47, 12590 (1993).
- [14] L. Y. Chen and C. S. Ting, *Phys. Rev. B* 43, 4534 (1991).
- [15] R. Lake and S. Datta, *Phys. Rev. B* 45, 6670 (1992).
- [16] R. Lake and S. Datta, *Phys. Rev. B* 46, 4757 (1992).
- [17] A. L. Yeyati, F. Flores, and E. V. Anda, *Phys. Rev. B* 47, 10543 (1993).
- [18] G. Kim, H. Suh, and E. Lee, *Phys. Rev. B* 52, 2632 (1995).
- [19] G. Klimeck, R. Lake, R. C. Bowen, W. R. Frensley, and T. Moise, *Appl. Phys. Lett.* 67, 2539 (1995).
- [20] R. Lake, G. Klimeck, R. C. Bowen, C. Fernando, M. Leng, T. Moise, and Y. C. Kao, *Superlatt. and Microstruct.* 20, 279 (1996).
- [21] R. Lake, G. Klimeck, R. C. Bowen, C. L. Fernando, D. Jovanovic, D. Blanks, T. S. Moise, Y. C. Kao, M. Leng, and W. R. Frensley, 1996 55th Annual Device Research Conference Digest (IEEE, New York, 1996), p. 174.
- [22] G. Klimeck, R. C. Bowen, T. Boykin, R. Lake, D. Blanks, T. S. Moise, Y. C. Kao, and W. R. Frensley, 1997 55th Annual Device Research Conference Digest (IEEE, New York, 1997), p. 92.
- [23] R. C. Bowen, G. Klimeck, R. K. Lake, W. R. Frensley, and T. Moise, *J. Appl. Phys.* 81, 3207 (1997).
- [24] M. J. McLennan, Y. Lee, and S. Datta, *Phys. Rev. B* 43, 13846 (1991).
- [25] S.-C. Lee and A. Wacker, *Phys. Rev. B* 66, 245314/1 (2002).
- [26] C. Rivas, R. Lake, G. Klimeck, W. R. Frensley, M. V. Fischetti, P. E. Thompson, S. L. Rommel, and P. R. Berger, *Appl. Phys. Lett.* 78, 814 (2001).
- [27] C. Rivas, R. Lake, W. R. Frensley, G. Klimeck, P. E. Thompson, K. D. Hobart, S. L. Rommel, and P. R. Berger, *J. Appl. Phys.* 94, 5005 (2003).
- [28] D. Jovanovic and R. Venugopal, in *7th International Workshop on Computational Electronics. Book of Abstracts (IWC E, Glasgow, 2000)*, p. 30.
- [29] A. Svizhenko, M. P. Anantram, T. R. Govindan, B. Biegel, and R. Venugopal, *J. Appl. Phys.* 91, 2343 (2002).
- [30] R. Lake, D. Jovanovic, and C. Rivas, *Progress in Nonequilibrium Green Functions* (World Scientific, New Jersey, 2003), pp. 143{158.
- [31] A. Svizhenko and M. P. Anantram, *IEEE Trans. Elect. Dev.* 50, 1459 (2003).
- [32] R. Venugopal, M. Paulsson, S. G. Dasgupta, S. Datta, and M. S. Lundstrom, *J. Appl. Phys.* 93, 5613 (2003).
- [33] Y.-J. Ko, M. Shin, S. Lee, and K. W. Park, *J. Appl. Phys.* 89, 374 (2001).
- [34] C. Rivas and R. Lake, in *Nanotech 2003 v. 2 Technical Proceedings of the 2003 Nanotechnology Conference and Trade Show* (Computational Publications, San Francisco, 2003), pp. 137{140.
- [35] C. Rivas and R. Lake, *phys. stat. sol. (b)* 239, 94 (2003).
- [36] M. B. Nardelli, *Phys. Rev. B* 60, 7828 (1999).
- [37] J. Taylor, H. Guo, and J. Wang, *Phys. Rev. B* 63, 245407/1 (2001).
- [38] H. M. Hertz, J. Taylor, H. Guo, J. Wang, and C. Roland, *Phys. Rev. Lett.* 84, 2682 (2000).
- [39] D. Orlikowski, H. M. Hertz, J. Taylor, H. Guo, J. Wang, and C. Roland, *Phys. Rev. B* 63, 155412/1 (2001).
- [40] J. Taylor, H. Guo, and J. Wang, *Phys. Rev. B* 63, 121104R/1 (2001).
- [41] M. P. Anantram, *Appl. Phys. Lett.* 78, 2005 (2001).
- [42] A. Maiti, A. Svizhenko, and M. P. Anantram, *Phys. Rev. Lett.* 88, 126805(4) (2002).
- [43] C.-C. Kuan, B. Larade, H. M. Hertz, J. Taylor, and H. Guo, *Phys. Rev. B* 65, 205416/1 (2002).
- [44] G. Cuniberti, R. Gutierrez, G. Fagas, F. Grossmann, K. Richter, and R. Schmidt, *Physica E* 12, 749 (2002).
- [45] J. J. Palacios, A. J. P. Jimenez, E. Louis, E. SanFabian, and J. Verges, *Phys. Rev. Lett.* 90, 106801(4) (2003).
- [46] Y. Xue and M. A. Ratner, *Appl. Phys. Lett.* 83, 2429 (2003).
- [47] T.-S. Xia, L. F. Register, and S. K. Banerjee, *J. Appl. Phys.* 95, 1597 (2004).
- [48] M. Brandbyge, J.-L. Mozos, P. Ordejon, J. Taylor, and K. Stokbro, *Phys. Rev. B* 65, 165401/1 (2002).
- [49] E. Louis, J. A. Verges, J. J. Palacios, A. J. Perez-Jimenez, and E. SanFabian, *Phys. Rev. B* 67, 155321/1 (2003).
- [50] W. Tian, S. Datta, S. Hong, R. Reifenberger, J. I. Henderson, and C. P. Kubiak, *J. Chem. Phys.* 109, 2874 (1998).
- [51] P. A. Derosa and J. M. Seminario, *J. Phys. Chem. B* 105, 471 (2001).
- [52] Y. Xue, S. Datta, and M. A. Ratner, *J. Chem. Phys.* 115, 4292 (2001).
- [53] Y. Xue, Ph.D. thesis, Purdue University (2000).

- [54] P. S. Damle, A. W. Ghosh, and S. Datta, *Phys. Rev. B* 64, 201403 (2001).
- [55] J. M. Seminario, A. G. Zacarias, and P. A. Derosa, *J. Phys. Chem. A* 105, 791 (2001).
- [56] J. M. Seminario and P. A. Derosa, *J. Am. Chem. Soc.* 123, 12418 (2001).
- [57] J. Taylor, M. Brandbyge, and K. Stokbro, *Phys. Rev. Lett.* 89, 138301/1 (2002).
- [58] J. Palacios, E. Louis, A. J. P. Jimenez, E. SanFabio, and J. Verges, *Nanotechnology* 13, 378 (2002).
- [59] J. Heinrich, J. C. Cuevas, W. Wenzel, and G. Schon, *Phys. Rev. Lett.* 88, 256803 (2002).
- [60] E. Louis, J. A. Verges, J. J. Palacios, A. J. P. Jimenez, and E. SanFabio, *Phys. Rev. B* 67, 155321 (5) (2003).
- [61] Y. Xue and M. A. Ratner, *Phys. Rev. B* 68, 115406(18) (2003).
- [62] J. M. Seminario, L. E. Cordova, and P. A. Derosa, *Proc. IEEE* 91, 1958 (2003).
- [63] M. Galperin, A. Nitzan, S. Sek, and M. Majla, *J. Electroanal. Chem.* 550, 337 (2003).
- [64] P. A. Derosa, S. Guda, and J. M. Seminario, *J. Am. Chem. Soc.* 125, 14240 (2003).
- [65] Y. Xue and M. A. Ratner, *Phys. Rev. B* 69, 085403(5) (2004).
- [66] A. W. Ghosh, T. Rakshit, and S. Datta, *Nanoletters* 4, 565 (2004).
- [67] F. Evers, F. W. Eigend, and M. Koenig, *Phys. Rev. B* 69, 235411/1 (2004).
- [68] U. G. S. N. E. and A. D. Zaikin, *Phys. Rev. B* 50, 6317 (1994).
- [69] W. I. Babiacyk and B. R. Bulka, *J. Phys.: Condens. Matter* 16, 4001 (2004).
- [70] S. Krompiecki, *J. Phys.: Condens. Matter* 16, 2981 (2004).
- [71] C. Caroli, R. Combescot, P. Nozieres, and D. Saint-James, *J. Phys. C: Solid State Physics* 4, 916 (1971).
- [72] M. A. Davydovich, E. V. Anda, C. Tejedor, and G. Platero, *Phys. Rev. B* 47, 4475 (1993).
- [73] G. Klimeck, R. Lake, and D. K. Banks, *Phys. Rev. B* 58, 7279 (1998).
- [74] Y. Xue, S. Datta, and M. A. Ratner, *Chemical Physics* 281, 151 (2002).
- [75] A. G. Roshev, T. Ivanov, and V. Valtchinov, *Phys. Rev. Lett.* 66, 1082 (1991).
- [76] L. Y. Chen and C. S. Ting, *Phys. Rev. B* 44, 5916 (1991).
- [77] S. Hershfeld, J. Davies, and J. Wilkins, *Phys. Rev. Lett.* 67, 3720 (1991).
- [78] S. Hershfeld, J. Davies, and J. Wilkins, *Phys. Rev. B* 46, 7046 (1992).
- [79] Y. M. eir, N. S. W. Ingreen, and P. A. Lee, *Phys. Rev. Lett.* 70, 2601 (1993).
- [80] N. S. W. Ingreen and Y. M. eir, *Phys. Rev. B* 49, 11040 (1994).
- [81] Y. Xue and M. A. Ratner, *Phys. Rev. B* 68, 235410/1 (2003).
- [82] S. Hershfeld, *Phys. Rev. B* 46, 7061 (1992).
- [83] S. Datta and M. P. A. Nantram, *Phys. Rev. B* 45, 13761 (1992).
- [84] M. P. A. Nantram and S. Datta, *Phys. Rev. B* 51, 7632 (1995).
- [85] N. S. W. Ingreen, A. Jauho, and Y. M. eir, *Phys. Rev. B* 48, 8487 (1993).
- [86] A. Jauho, N. S. W. Ingreen, and Y. M. eir, *Phys. Rev. B* 50, 5528 (1994).
- [87] C. A. Staord and N. S. W. Ingreen, *Phys. Rev. Lett.* 76, 1916 (1996).
- [88] P. Kral, *Phys. Rev. B* 53, 11034 (1996).
- [89] P. Kral and A. P. Jauho, *Phys. Rev. B* 59, 7656 (1999).
- [90] H. Haug and A. P. Jauho, *Quantum kinetics in transport and optics of semiconductors*, vol. Springer Series in Solid-State Sciences, vol. 123 (Springer, Berlin, 1996).
- [91] S. Datta, *Electronic Transport in Mesoscopic Systems* (Cambridge University Press, New York, 1995).
- [92] S. Datta, *Superlatt. Microstruct.* 28, 253 (2000).
- [93] C. Caroli, R. Combescot, D. Lederer, P. Nozieres, and D. Saint-James, *J. Phys. C: Solid St. Phys.* 4, 2598 (1971).
- [94] R. Combescot, *J. Phys. C: Solid St. Phys.* 4, 2611 (1971).
- [95] C. Caroli, R. Combescot, P. Nozieres, and D. Saint-James, *J. Phys. C: Solid State Physics* 5, 21 (1972).
- [96] W. R. Bandy and A. J. Glick, *Phys. Rev. B* 13, 3368 (1976).
- [97] W. R. Bandy and A. J. Glick, *Phys. Rev. B* 16, 2346 (1977).
- [98] M. Cini, *Phys. Rev. B* 22, 5887 (1980).
- [99] C. B. Duke, *Tunneling in Solids* (Academic Press, New York, 1969).
- [100] D. K. Banks, G. Klimeck, R. Lake, D. Jovanovic, R. C. Bowen, C. Fernando, W. R. Frensley, and M. Leng, in *Compound Semiconductors 1997. Proceedings of the IEEE Twenty-Fourth International Symposium on Compound Semiconductors* (IEEE, New York, 1998), pp. 639-642.
- [101] R. Lake, G. Klimeck, R. Bowen, D. Jovanovic, P. Sotirelis, and W. R. Frensley, *VLSI Design* 6, 9 (1998).
- [102] R. Lake, G. Klimeck, and D. K. Banks, *Semicond. Sci. Technol.* 13, A163 (1998).
- [103] N. Zou, M. Willander, I. Linnerud, U. Hanke, K. A. Chao, and Y. M. Galperin, *Phys. Rev. B* 49, 2193 (1994).
- [104] T. P. E. Broekaert, W. Lee, and C. G. Fonstad, *Appl. Phys. Lett.* 53, 1545 (1988).
- [105] B. Brar, G. D. Wilks, and A. C. Seabaugh, *Appl. Phys. Lett.* 69, 2728 (1996).
- [106] S. L. Rommel, T. E. Dillon, M. W. Dashiell, H. Feng, J. Koldzay, P. R. Berger, P. E. Thompson, K. D. Hobart, R. Lake, A. Seabaugh, et al., *Appl. Phys. Lett.* 73, 2191 (1998).
- [107] G. D. Mahan, *Many-Particle Physics* (Plenum, New York, 1990), 2nd ed.
- [108] T. B. Boykin, *Phys. Rev. B* 60, 15810 (1999).
- [109] D. C. Langreth, *Linear and Non-linear Electron Transport in Solids*, NATO ASI Series, Vol. 17 (Plenum, New York, 1976).
- [110] S. Hershfeld, *Phys. Rev. Lett.* 70, 2134 (1993).
- [111] R. A. Craig, *J. Math. Phys.* 9, 605 (1968).
- [112] A. L. Fetter and J. D. Walecka, *Quantum Theory of Many-Particle Systems* (McGraw-Hill, New York, 1971).

- [113] P. Hyldgaard, S. Hershfeld, J. H. Davies, and J. W. Wilkins, *Ann. Phys.* 236, 1 (1994).
- [114] B. K. Ridley, *Quantum Processes in Semiconductors* (Oxford University Press, New York, 1988), 2nd ed.
- [115] R. Lake, in 2001 IEDM Technical Digest (IEEE, New York, 2001), pp. 5.5.1 { 5.5.4.
- [116] <http://www-hpc.jplnasa.gov/PEP/gekco/nemoid/index.html>.
- [117] T. B. Boykin, *Phys. Rev. B* 54, 8107 (1996).
- [118] J.-M. Jancu, R. Scholz, F. Beltram, and F. Bassani, *Phys. Rev. B* 57, 6493 (1998).
- [119] D. S. Fisher and P. A. Lee, *Phys. Rev. B* 23, 6851 (1981).
- [120] P. M. Solomon, J. Jopling, D. J. Frank, C. D'Emic, O. Dokumaci, P. Ronsheim, and W. E. Haensch, *J. Appl. Phys.* 95, 5800 (2004).
- [121] A. Wacker and A.-P. Jauho, *Phys. Rev. Lett.* 83, 836 (1999).
- [122] A. Wacker, *Phys. Rev. B* 66, 085326/1 (2002).
- [123] A. Wacker, *Phys. Rep.* 357, 1 (2002).
- [124] R. Venugopal, Z. Ren, S. Datta, and M. S. Lundstrom, *J. Appl. Phys.* 92, 3730 (2002).
- [125] M. Lundstrom and Z. Ren, *IEEE Trans. Electron. Dev.* 49, 133 (2002).
- [126] D. A. Antoniadis, I. J. Djmehri, K. M. Jackson, and S. Miller, "<http://www-mtl.mit.edu/Well/>".
- [127] The algorithm was developed by D. Jovanovic.
- [128] T. B. Boykin, G. Klimeck, and F. Oyafuso, *Phys. Rev. B* 69, 115201/1 (2004).
- [129] M. P. A nantram and T. R. Govindan, *Phys. Rev. B* 58, 4882 (1998).
- [130] M. P. A nantram and T. R. Govindan, *Phys. Rev. B* 61, 5020 (2000).
- [131] J. Guo, S. Datta, and M. Lundstrom, *IEEE Trans. Electron. Dev.* 51, 172 (2004).
- [132] R. Saito, G. Dresselhaus, and M. S. Dresselhaus, *Physical Properties of Carbon Nanotubes* (Imperial College Press, London, 1998).
- [133] K. Stokbro, J. Taylor, M. Brandbyge, and P. Ordejon, *Molecular Electronics III Ann. of the New York Acad. of Sci.* 1006, 212 (2003).
- [134] X. Zhang, L. Fonseca, and A. A. Demkov, *Phys. Stat. Sol. (b)* 233, 70 (2002).
- [135] A. Szabo and N. S. Ostlund, *Modern Quantum Chemistry: Introduction to Advanced Electronic Structure Theory* (Macmillan, New York, 1982).
- [136] J. Lindbergh and Y. Ohm, *Propagators in Quantum Chemistry* (Academic Press, New York, 1973).
- [137] A. A. Stuchebrukhov, *Chem. Phys. Lett.* 265, 643 (1997).
- [138] P. C. P. de Andrade and J. A. Freire, *J. Chem. Phys.* 118, 6733 (2003).
- [139] D. Lohez and M. Lannoo, *Phys. Rev. B* 27, 5007 (1983).
- [140] A. R. Williams, P. J. Feibelman, and N. D. Lang, *Phys. Rev. B* 26, 5433 (1982).
- [141] H. Ehrenreich, F. Seitz, and D. Turnbull, eds., vol. 35 of *Solid State Physics, Advances in Research and Applications* (Academic Press, New York, 1980).
- [142] W. Harrison, *Elementary Electronic Structure* (World Scientific, New Jersey, 1999).
- [143] P. Fulde, *Electron Correlations in Molecules and Solids* (Springer-Verlag, Berlin, 1993), 2nd ed.
- [144] P. E. A. Turchi, A. Gonis, and L. Colombo, eds., *Tight-Binding Approach to Computational Materials Science*, vol. 491 of *Materials Research Society Symposium Proceedings* (Mat. Res. Soc., Warrendale, PA, 1998).
- [145] J. Inglesfeld, *Computer Physics Communications* 137, 89 (2001).
- [146] R. P. Feynman, *Statistical Mechanics: A set of Lectures* (Addison-Wesley, New York, 1988).
- [147] F. Evers, F. W. E. G. and M. Koenig, *Phys. Rev. B* 69, 235411/1 (2004).
- [148] Y. Meir and N. Wingreen, *Phys. Rev. Lett.* 68, 2512 (1992).
- [149] W. H. Press, S. A. Teukolsky, W. T. Vetterling, and B. P. Flannery, *Numerical Recipes in Fortran, The Art of Scientific Computing* (Cambridge University Press, Cambridge, 1992), 2nd ed., p. 70.
- [150] We note in passing that Wicke's theorem applies as usual to the operators representing a non-orthogonal basis. This can be seen by performing the expansion using the field operators  $\psi(r)$  and  $\psi^\dagger(r)$  and then integrating over  $r$ .
- [151] This assumes that the orbitals associated with atom 0 are in equilibrium. This may no longer be the case since the contact is now defined as a region of space rather than a set of orbitals.
- [152] L. C. L. Y. Voon and L. R. Ram-Mohan, *Phys. Rev. B* 47, 15500 (1993).
- [153] M. Graf and P. Vogl, *Phys. Rev. B* 51, 4940 (1995).
- [154] T. B. Boykin and P. Vogl, *Phys. Rev. B* 65, 035202/1 (2001).
- [155] This argument was formulated by A. Kurotkov (private communication).
- [156] N. S. Wingreen, K. W. Jakobsen, and J. W. Wilkins, *Phys. Rev. B* 40, 11834 (1989).
- [157] P. E. Thompson, K. D. Hobart, M. E. Twigg, G. G. Jemigan, T. E. Dillon, S. L. Rommel, P. R. Berger, D. S. Simons, P. H. Chi, R. Lake, et al., *Appl. Phys. Lett.* 75, 1308 (1999).

## Figure C captions

1. Example calculation including incoherent scattering from acoustic phonons, polar optical phonons and interface roughness. The simulations are compared against experimental data. Reprinted from [21]. Copyright 1996 IEEE.
2. Test matrix of  $\text{In}_{0.47}\text{Ga}_{0.53}\text{As}$  /  $\text{AlAs}$  RTDs. The collector barrier is increased by one monolayer for the 3 RTDs from left to right. Forward and reverse bias current voltage curves are shown and overlaid on experimental data. Reprinted from [22]. Copyright 1997 IEEE.
3. Test matrix of  $\text{In}_{0.47}\text{Ga}_{0.53}\text{As}$  /  $\text{In}_{0.48}\text{Al}_{0.52}\text{As}$  RTDs. (a-c) The well thickness is increased. (c-f) the undoped spacer layer is increased. Reprinted from [22]. Copyright 1997 IEEE.
4. Experimental data and simulation of the capacitance - voltage curve of a MOS structure with a 3.1 nm oxide. Reprinted from [115]. Copyright 2001 IEEE.
5. Simulation of band profile of the  $\text{Si}/\text{Si}_{0.5}\text{Ge}_{0.5}$  tunnel diode. Reprinted from [106].
6. Band profile of the delta-doped Si tunnel diode biased at 0.1V. Inset, 6 X valleys of the conduction band. Reprinted from [26].
7. Three current components: TA phonon assisted, TO phonon assisted, and direct or coherent current. Inset, 2D electron and hole dispersions. Reprinted from [26].
8. Experimental I-V from ref. [157] corrected for lead series resistance overlaid on calculated I-Vs with different energy broadening in the contacts as shown in the legend. Reprinted from [27].
9. Comparison of the real and imaginary dispersion relations calculated (a) from the parabolic single band model using the transverse conduction band mass of  $0.19 m_0$  and from the full-band model in the transverse mass direction of the  $X_4$  conduction band valley and (b) from the single band model using the light hole mass of  $0.16 m_0$  and from the full-band model in the valence band in the (001) direction. The horizontal axis to the left of 0 is imaginary  $k$  and to the right of 0 is real  $k$ . Reprinted from [27].
10. Quantum cascade laser structure modeled in [25]. Reprinted with permission from [25]. Copyright 2002 American Physical Society.
11. Drain current and channel barrier height versus extent of scattering region (starting from source at -20 nm). Inset:  $I_D$  vs.  $V_D$  curves for  $V_G = 0.6$  V. Reprinted with permission from [31]. Copyright 2003 IEEE.
12. Self-energy diagram for self-consistent Born approximation.
13. Keldysh time contour.

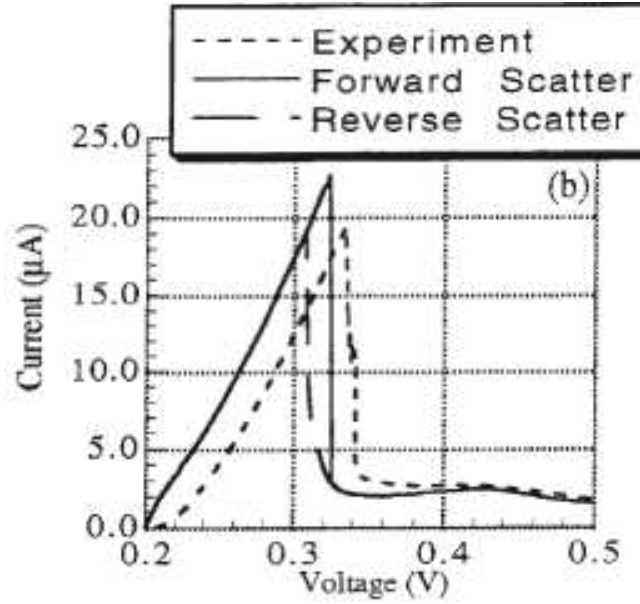


FIG . 1 : Exam ple calculation including incoherent scattering from acoustic phonons, polar optical phonons and interface roughness. The simulations are compared against experimental data. Reprinted from [21]. Copyright 1996 IEEE .

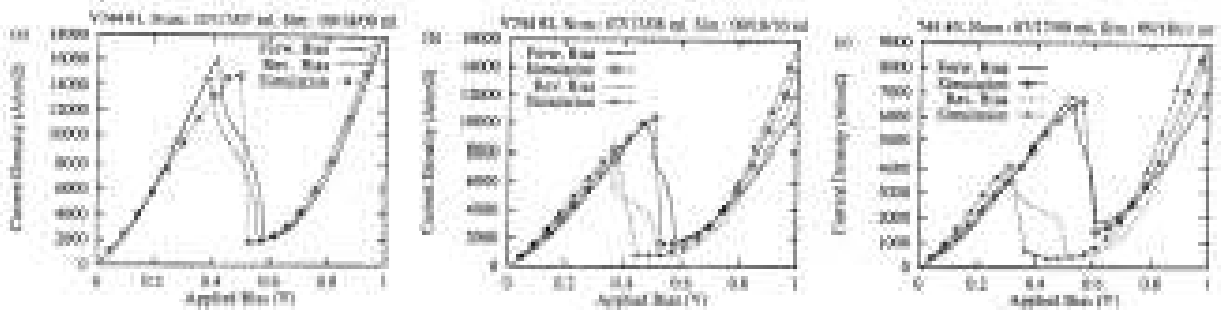


FIG . 2 : Test matrix of  $In_{0.47}Ga_{0.53}As / AlAs$  RTDs. The collector barrier is increased by one monolayer for the 3 RTDs from left to right. Forward and reverse bias current voltage curves are shown and overlaid on experimental data. Reprinted from [22]. Copyright 1997 IEEE .



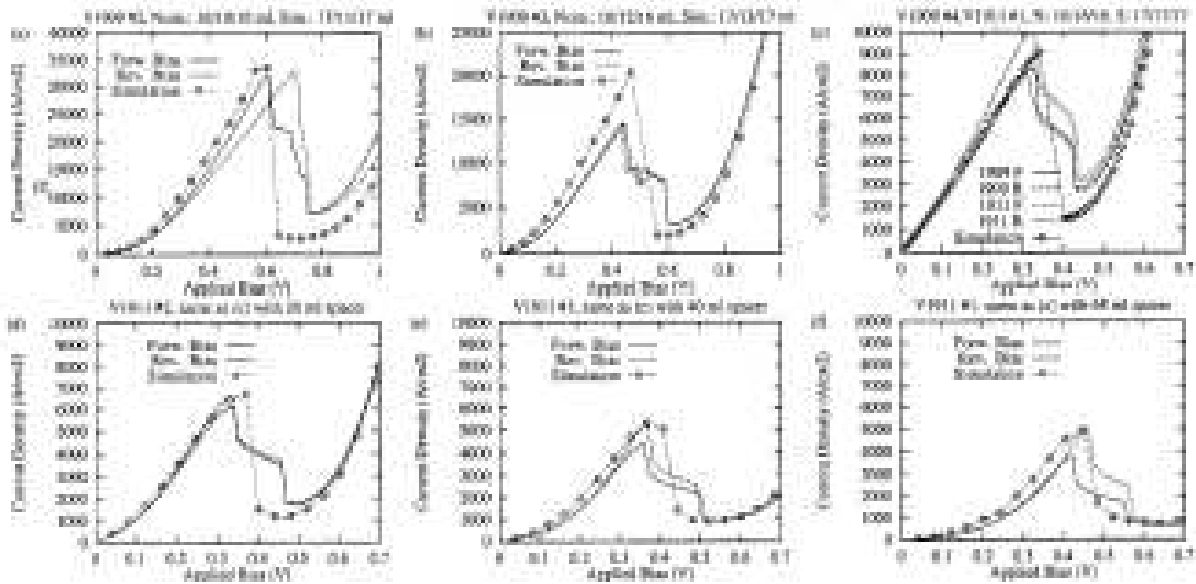


FIG. 3: Test matrix of  $\text{In}_{0.47}\text{Ga}_{0.53}\text{As} / \text{In}_{0.48}\text{Al}_{0.52}\text{As}$  RTDs. (a-c) The well thickness is increased. (c-f) the undoped spacer layer is increased. Reprinted from [22]. Copyright 1997 IEEE.

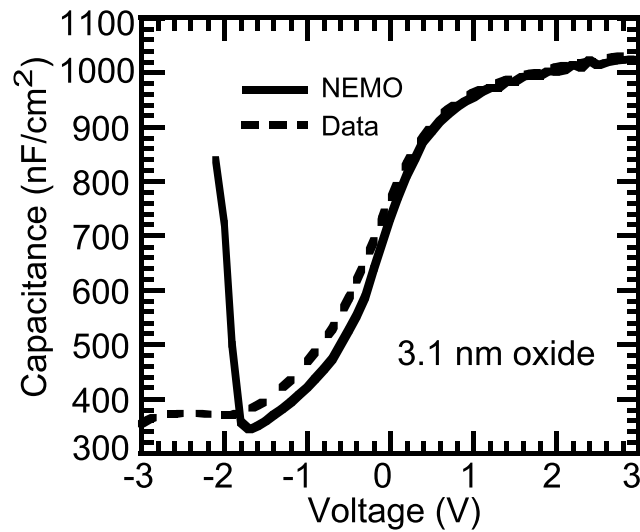


FIG. 4: Experimental data and simulation of the capacitance-voltage curve of a MOS structure with a 3.1 nm oxide. Reprinted from [15]. Copyright 2001 IEEE.

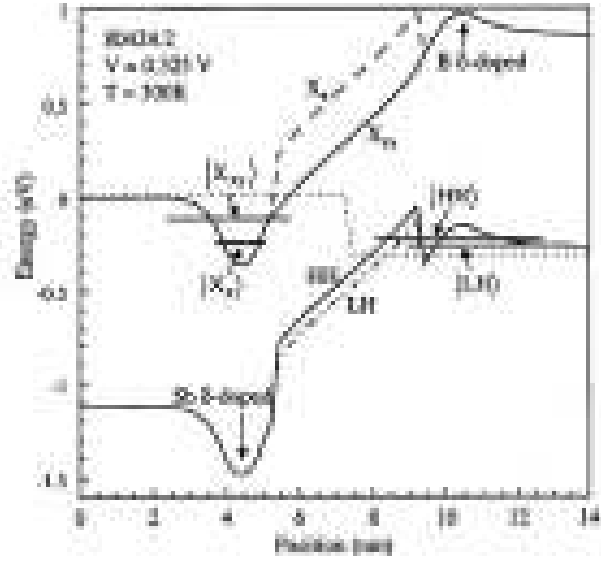


FIG . 5: Simulation of band profile of the Si/ Si<sub>0.5</sub>Ge<sub>0.5</sub> tunnel diode. Reprinted from [106].

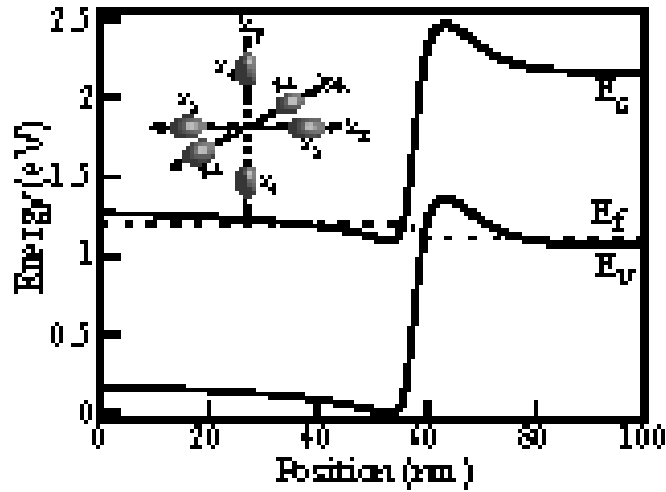


FIG . 6: Band profile of the delta-doped Si tunnel diode biased at 0.1V . Inset, 6 X valleys of the conduction band. Reprinted from [26].

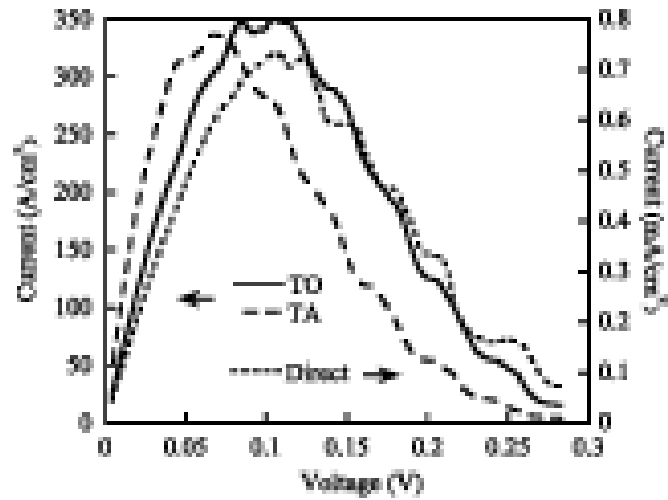


FIG .7: Three current components: TA phonon assisted, TO phonon assisted, and direct or coherent current. Inset, 2D electron and hole dispersions. Reprinted from [26].

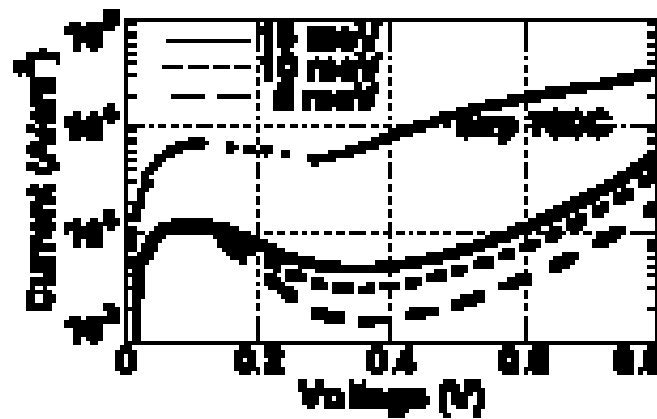


FIG .8: Experimental I-V from ref. [157] corrected for 12  $\Omega$  series resistance overlaid on calculated I-Vs with different energy broadenings in the contacts as shown in the legend. Reprinted from [27].

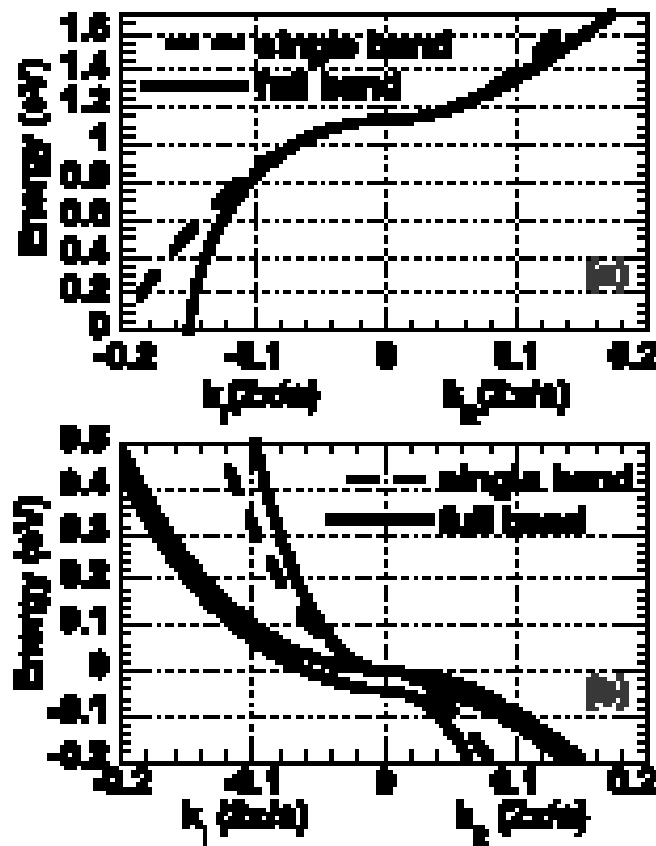


FIG. 9: Comparison of the real and imaginary dispersion relations calculated (a) from the parabolic single band model using the transverse conduction band mass of  $0.19 m_0$  and from the full-band model in the transverse mass direction of the  $X_4$  conduction band valley and (b) from the single band model using the light hole mass of  $0.16 m_0$  and from the full-band model in the valence band in the (001) direction. The horizontal axis to the left of 0 is imaginary  $k$  and to the right of 0 is real  $k$ . Reprinted from [27].

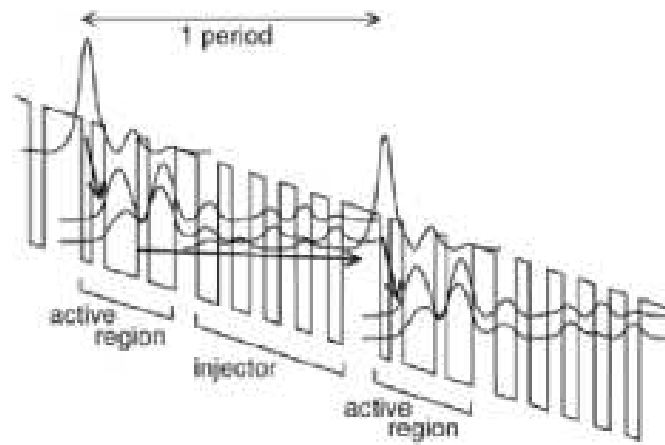


FIG . 10: Quantum cascade laser structure modeled in [25]. Reprinted with permission from [25]. Copyright 2002 American Physical Society.

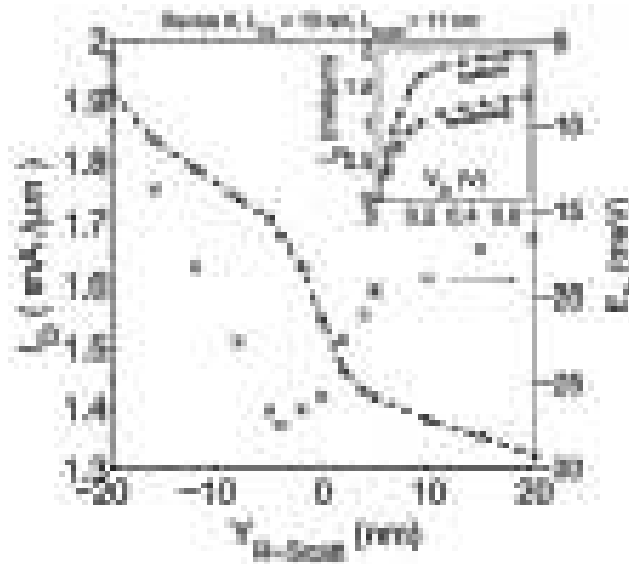


FIG . 11: Drain current and channel barrier height versus extent of scattering region (starting from source at -20 nm). Inset:  $I_D$  vs.  $V_D$  S curves for  $V_G = 0.6$  V. Reprinted with permission from [31]. Copyright 2003 IEEE.

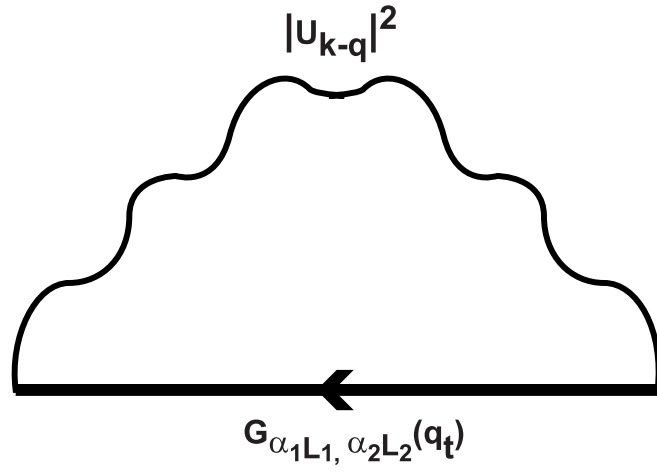


FIG . 12: Self-energy diagram for self-consistent Born approximation.

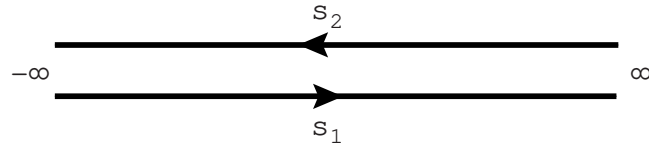


FIG . 13: Keldysh time contour.